

This is a repository copy of *Propagation of Beta/Gamma Rhythms in the Cortico-Basal Ganglia Circuits of the Parkinsonian Rat*.

White Rose Research Online URL for this paper:

<https://eprints.whiterose.ac.uk/126703/>

Version: Accepted Version

Article:

West, Timothy Owen, Berthouze, Luc, Halliday, David M orcid.org/0000-0001-9957-0983 et al. (4 more authors) (2018) Propagation of Beta/Gamma Rhythms in the Cortico-Basal Ganglia Circuits of the Parkinsonian Rat. *Journal of Neurophysiology*. pp. 1608-1628. ISSN 0022-3077

<https://doi.org/10.1152/jn.00629.2017>

Reuse

Items deposited in White Rose Research Online are protected by copyright, with all rights reserved unless indicated otherwise. They may be downloaded and/or printed for private study, or other acts as permitted by national copyright laws. The publisher or other rights holders may allow further reproduction and re-use of the full text version. This is indicated by the licence information on the White Rose Research Online record for the item.

Takedown

If you consider content in White Rose Research Online to be in breach of UK law, please notify us by emailing eprints@whiterose.ac.uk including the URL of the record and the reason for the withdrawal request.

1 Propagation of Beta/Gamma Rhythms in 2 the Cortico-Basal Ganglia Circuits of the 3 Parkinsonian Rat

4 Timothy O. West^{1,2*}, Luc Berthouze^{3,4}, David M. Halliday⁵, Vladimir Litvak²,
5 Andrew Sharott⁶, Peter J. Magill^{6,7}, Simon F. Farmer^{8,9}

6 ¹*CoMPLEX, Centre for Mathematics and Physics in the Life Sciences and Experimental Biology, UCL*
7 *Department of Physics and Astronomy, Gower Street, London, WC1E 6BT*

8 ²*Wellcome Trust Centre for Neuroimaging, UCL Institute of Neurology, Queen Square, London,*
9 *WC1N 3BG*

10 ³*Centre for Computational Neuroscience and Robotics, University of Sussex, Falmer, UK*

11 ⁴*UCL Great Ormond Street Institute of Child Health, Guildford St., London, WC1N 1EH*

12 ⁵*Department of Electronic Engineering, University of York, YO10 5DD, UK.*

13 ⁶*Medical Research Council Brain Network Dynamics Unit, University of Oxford, Oxford, OX1 3TH,*
14 *United Kingdom.*

15 ⁷*Oxford Parkinson's Disease Centre, University of Oxford, Oxford OX1 3QX, United Kingdom.*

16 ⁸*Department of Neurology, National Hospital for Neurology & Neurosurgery, Queen Square, London*
17 *WC1N 3BG*

18 ⁹*Sobell Department of Motor Neuroscience and Movement Disorders, Institute of Neurology, UCL,*
19 *London WC1N 3BG.*

20 **Corresponding Author*

21 Abstract

22 Much of the motor impairment associated with Parkinson's disease is thought to arise from
23 pathological activity in the networks formed by the basal ganglia (BG) and motor cortex. To evaluate
24 several hypotheses proposed to explain the emergence of pathological oscillations in Parkinsonism,
25 we investigated changes to the directed connectivity in BG networks following dopamine depletion.

26 We recorded local field potentials (LFPs) in the cortex and basal ganglia of rats rendered Parkinsonian
27 by injection of 6-hydroxydopamine (6-OHDA) and in dopamine-intact controls. We performed
28 systematic analyses of the networks using a novel tool for estimation of directed interactions (Non-
29 Parametric Directionality, NPD). We used a ‘conditioned’ version of the NPD analysis which reveals
30 the dependence of the correlation between two signals upon a third reference signal. We find evidence
31 of the dopamine dependency of both low beta (14-20 Hz) and high beta/low gamma (20-40 Hz)
32 directed network interactions. Notably, 6-OHDA lesions were associated with enhancement of the
33 cortical “hyper-direct” connection to the subthalamic nucleus (STN) and its feedback to the cortex
34 and striatum. We find that pathological beta synchronization resulting from 6-OHDA lesioning is
35 widely distributed across the network and cannot be located to any individual structure. Further, we
36 provide evidence that high beta/gamma oscillations propagate through the striatum in a pathway that
37 is independent of STN. Rhythms at high beta/gamma show susceptibility to conditioning that
38 indicates a hierarchical organization when compared to low beta. These results further inform our
39 understanding of the substrates for pathological rhythms in salient brain networks in Parkinsonism.

40 Keywords

41 Parkinson’s disease; basal ganglia; local field potential; synchronization; connectivity;

42 New & Noteworthy

43 We present a novel analysis of electrophysiological recordings in the cortico-basal ganglia network
44 with the aim of evaluating several hypotheses concerning the origins of abnormal brain rhythms
45 associated with Parkinson’s disease. We present evidence for changes in the directed connections
46 within the network following chronic dopamine depletion in rodents. These findings speak to the
47 plausibility of a “short-circuiting” of the network that gives rise to the conditions from which
48 pathological synchronization may arise.

49 Introduction

50 The basal ganglia (BG) are host to a small but important cluster of dopaminergic neurons that act to
51 modulate the activity of a large re-entrant network that comprises the cortico-basal ganglia-thalamo-
52 cortical circuit (DeLong and Wichmann 2010; Lanciego et al. 2012). Investigation of the structure of
53 this network (Smith et al. 1998; Bolam et al. 2000) has led to what has become a canonical view of
54 the circuit (depicted in Figure 1A) and has formed the basis from which a number of process theories
55 of BG function have arisen (for a review, see Schroll and Hamker, (2013)).

56 Recent theory concerning the organisation of brain networks and communication within them via
57 synchronized oscillations (Varela et al. 2001; Fries 2005, 2015; Bressler and Menon 2010; Thut et al.
58 2012) has emphasised the importance of understanding the dynamics of these networks beyond that
59 afforded by studying structural connectivity alone (Deco et al. 2008, 2012). Neural oscillations and

60 their synchronization have been measured across multiple spatial scales of brain activity, from single
61 neuronal discharges up to the level of mesoscale neural ensembles such as those measured in the local
62 field potential (LFP) or electrocorticogram (ECoG). Moreover, dysregulations of oscillations and
63 inter-areal synchrony have been reported in brain disorders such as Parkinson's disease (PD),
64 schizophrenia, and epilepsy, leading to the hypothesis that the oscillations themselves bear a causal
65 role in the behavioral impairments associated with these pathologies (Schnitzler and Gross 2005;
66 Uhlhaas and Singer 2006; Hammond et al. 2007).

67 Excessive beta oscillations (14-30 Hz) in the BG associated with dopamine depletion have been
68 observed reliably in untreated patients with PD (Levy et al. 2000; Brown et al. 2001; Weinberger et
69 al. 2006; Hammond et al. 2007). Beta rhythms are attenuated by treatments such as dopamine
70 replacement therapy (Kühn et al. 2006; Weinberger et al. 2006; West et al. 2016; Beudel et al. 2017;
71 Levy 2002) and deep brain stimulation (DBS) (Ray et al. 2008; Eusebio et al. 2011; Whitmer et al.
72 2012) in a way that correlates with the degree of improvement of akinetic/rigid motor symptoms. This
73 has strengthened the argument that the pathological beta rhythms are directly related to the functional
74 impairment seen in patients (Hanslmayr et al. 2012; Brittain and Brown 2014). Furthermore, gamma
75 activity in the motor system has been hypothesized to be prokinetic (Schoffelen et al. 2005). In PD,
76 the spectral power of multiunit recordings from STN at 40-90 Hz have been demonstrated to be
77 negatively correlated with bradykinetic symptoms in patients (Sharott et al. 2014).

78 The pathological oscillations observed in mesoscale electrophysiological signals are a direct
79 consequence of changes to the underlying networks of neuronal ensembles that generate them. This
80 understanding has led to the re-classification of multiple neurological diseases such as PD or
81 Tourette's as 'circuit disorders' (DeLong and Wichmann 2010). Knowledge of how dopamine
82 depletion results in changes to the network, and the subsequent emergence of pathological synchrony
83 is likely to lead to a better understanding of the causes of impairment and its treatments (Shen et al.
84 2008; Schroll et al. 2014). Thus, improving insight into how changes network organization leads to
85 the emergence of pathological dynamics is an important line of enquiry (Wichmann and DeLong
86 1999; Dostrovsky and Bergman 2004; Holgado et al. 2010)

87 Previous work aiming to understand the origins of the pathological beta rhythm has involved
88 systematic lesioning of the BG network (Ni et al. 2000; Tachibana et al. 2011), computational
89 modelling (Holgado et al. 2010; Moran et al. 2011; Marreiros et al. 2013; Nevado-Holgado et al.
90 2014; Pavlides et al. 2015; Lienard et al. 2017), and techniques from signal analysis (Sharott et al.
91 2005a; Mallet et al. 2008a, 2008b; Litvak et al. 2011a). In this paper, we take the latter approach and,
92 through analysis of neural recordings, aim to infer the changes in neural transmission that occur in
93 cortico-BG circuits following chronic dopamine depletion.

94 Connectivity between parts of the brain can be inferred from the statistical dependencies that arise due
95 to neural transmission: we refer to this as functional connectivity as per Friston (2011). Previous
96 studies have aimed to describe ‘effective’ connectivity (i.e. causal interactions) within this network
97 and have employed the dynamic causal modeling (DCM) framework in order to do so. To date, two
98 such studies have utilised the inversion of biophysical models upon cross spectral densities from
99 recordings in either anaesthetised 6-OHDA lesioned rats (Moran et al. 2011), or awake DBS patients
100 (Marreiros et al. 2013). Both found evidence for the strengthening of the cortico-subthalamic
101 connection (termed the ‘hyper-direct’ pathway (Nambu et al. 2002)) in the dopamine-depleted state.

102 From this work amongst others, several hypotheses have arisen concerning the emergence of
103 pathological beta rhythms as a result of the dopamine depletion associated with PD (for a review see
104 Holgado et al. 2010). These include the dopamine-dependent modulation of recurrent loops within the
105 network, either between the reciprocally-coupled network of neurons of the subthalamic nucleus
106 (STN) and the external globus pallidus (GPe) (Plenz and Kital 1999; Bevan et al. 2002; Terman et al.
107 2002; Holgado et al. 2010; Liu et al. 2017); or of a longer loop involving feedback from BG output
108 nuclei to the cortex via thalamo-cortical tracts (Leblois et al. 2006; Pavlides et al. 2012, 2015).
109 Alternatively, it has been proposed that dopamine depletion disrupts mechanisms which regulate the
110 gain of cortical afferents to the BG and somehow disrupt striatal outflow (Brown 2007; Hammond et
111 al. 2007). The striatum (STR) itself has also been implicated in the generation of pathological beta
112 rhythms, either through alterations to its internal dynamics (McCarthy et al. 2011; Damodaran et al.
113 2015); or via increased striatal inhibition of targets in the GPe that act to promote beta synchrony
114 (Gillies and Willshaw 2004; Kumar et al. 2011a).

115 Here, using a recently described non-parametric (model-free) signal analysis technique (Halliday et
116 al., 2015), we study the effects of dopamine depletion upon neural connectivity in the network formed
117 by elements of the BG and motor cortex in 6-OHDA-lesioned and dopamine-intact control rats. We
118 employ this method as a measure of *directed* functional connectivity (hereon shortened to directed
119 connectivity). It is a model-free estimate that makes no assumptions as to the causes of the data (for
120 discussion see Bastos and Schoffelen 2016), only that temporal precedence implies a driving neuronal
121 influence (please see later sections for discussion). Furthermore, we use a a multivariate extension of
122 the framework (Halliday et al. 2016) in order to determine whether the interaction between two areas
123 shares correlation with activity recorded at a third structure in the network. This approach provides
124 insight into frequency-specific directional connectivity and the degree to which transmission between
125 two coupled regions are autonomous of another reference region. By recording LFPs and ECoG in 6-
126 OHDA-lesioned animals and dopamine-intact controls we aim to identify changes to connectivity that
127 occur as a result of the loss of dopamine from these circuits. Our findings are interpreted within the
128 context of the canonical circuit (Figure 1A), as well as other existing models of basal ganglia

129 connectivity, and several hypotheses concerning the generation and propagation neural rhythms in the
130 network.

131 Methods

132 Experimental Data

133 Electrophysiological Recordings

134 Experimental procedures were carried out on adult male Sprague-Dawley rats (Charles River,
135 Margate, UK) and were conducted in accordance with the Animals (Scientific Procedures) Act, 1986
136 (UK). Recordings were made in eight dopamine-intact control rats (288–412 g) and nine 6-OHDA-
137 lesioned rats (285–428 g at the time of recording), as described previously (Magill et al. 2006; Mallet
138 et al. 2008a, 2008b; Moran et al. 2011). Briefly, anesthesia was induced with 4% v/v isoflurane
139 (Isoflo, Schering-Plough Ltd., Welwyn Garden City, UK) in O₂, and maintained with urethane (1.3
140 g/kg, i.p.; ethyl carbamate, Sigma, Poole, UK), and supplemental doses of ketamine (30 mg/kg;
141 Ketaset, Willows Francis, Crawley, UK) and xylazine (3 mg/kg; Rompun, Bayer, Germany).

142 The ECoG was recorded via a 1 mm diameter steel screw juxtaposed to the dura mater above the right
143 frontal cortex (centred at 4.5 mm anterior and 2.0 mm lateral of Bregma, corresponding to the
144 “secondary motor cortex” (M2) of (Paxinos and Watson 2007) or the medial agranular field of the
145 somatic sensorimotor cortex of Donoghue and Wise, (1982); see Figure 1B) and was referenced
146 against another screw implanted in the skull above the ipsilateral cerebellar hemisphere. Raw ECoG
147 was band-pass filtered (0.3–1500 Hz, -3 dB limits) and amplified (2000x; DPA-2FS filter/amplifier:
148 Scientifica Ltd., Harpenden, UK) before acquisition (see below). Extracellular recordings of LFPs in
149 the dorsal striatum (STR), GPe and STN were simultaneously made in each animal using ‘silicon
150 probes’ (NeuroNexus Technologies, Ann Arbor, MI); a first probe captured LFPs in STR and GPe,
151 whereas a second probe captured LFPs in the STN (Figure 1B). Each probe had one vertical array of
152 16 recording contacts (impedance of 0.9–1.3 M Ω measured at 1000 Hz; area of \sim 400 μ m²), and each
153 contact on a given probe was separated by 100 μ m. Recording sites in the BG were verified by post
154 hoc histology, as described previously (Magill et al. 2006; Mallet et al. 2008a, 2008b), as well as by
155 comparisons of recorded unit activity with the characteristic discharges of STR, GPe and STN
156 neurons in anesthetized dopamine-intact rats and 6-OHDA-lesioned rats (Magill et al. 2006; Mallet et
157 al. 2008a, 2008b; Abdi et al. 2015; Sharott et al. 2017). The same two probes were used throughout
158 these experiments, but were cleaned after each experiment in a proteolytic enzyme solution to ensure
159 that contact impedances and recording performance were not altered by probe use and re-use (Magill
160 et al. 2006; Sharott et al. 2017). Monopolar probe signals were recorded using high-impedance unity-
161 gain operational amplifiers (Advanced LinCMOS: Texas Instruments, Dallas, TX) and were
162 referenced against a screw implanted above the contralateral cerebellar hemisphere. After initial
163 amplification, extracellular signals were further amplified (1000x) and low-pass filtered at 6000 Hz

164 using programmable differential amplifiers (Lynx-8: Neuralynx, Tucson, AZ). The ECoG and probe
165 signals were each sampled at 17.9 kHz using a single Power1401 Analog-Digital converter (with
166 integrated ADC16 expansion units) and a PC running Spike2 acquisition and analysis software
167 (Cambridge Electronic Design Ltd., Cambridge, UK). All signals recorded in a given experimental
168 epoch were captured in a single data file. This, together with the use of a fixed/consistent sampling
169 rate and a single acquisition interface, ensured accurate synchronization (temporal alignment) of
170 cortical and BG signals.

171 Neuronal activity was recorded during episodes of spontaneous ‘cortical activation’, which contain
172 patterns of activity that are similar to those observed during the awake, behaving state (Steriade
173 2000). Cortical activation was defined according to ECoG activity. Neuronal activity patterns present
174 under this anesthetic regime may only be qualitatively similar to those present in the unanesthetized
175 brain. However, the urethane-anesthetized animal still serves as a useful model for assessing ensemble
176 dynamics within the basal ganglia. Indeed, in 6-OHDA-lesioned animals, exaggerated beta
177 oscillations emerge in cortico-basal ganglia circuits during activated brain states thus accurately
178 mimicking the oscillatory activity recorded in awake, un-medicated PD patients. Examples of the raw
179 electrophysiological signals as well the corresponding power spectra for control and lesioned animals
180 are shown in Figure 2.

181 6-Hydroxydopamine Lesions of Dopamine Neurons

182 Unilateral 6-OHDA lesions were carried out on 200–250 g rats, as described previously (Mallet et al.
183 2008a, 2008b). Twenty-five minutes before the injection of 6-OHDA, all animals received a bolus of
184 desipramine (25 mg/kg, i.p.; Sigma) to minimize the uptake of 6-OHDA by noradrenergic neurons
185 (Schwartz and Huston 1996a). Anesthesia was induced and maintained with 4% v/v isoflurane (see
186 above). The neurotoxin 6-OHDA (hydrochloride salt; Sigma) was dissolved immediately before use
187 in ice-cold 0.9% w/v NaCl solution containing 0.02% w/v ascorbate to a final concentration of 4
188 mg/ml. Then 3 ml of 6-OHDA solution was injected into the region adjacent to the medial substantia
189 nigra (4.5 mm posterior and 1.2 mm lateral of Bregma, and 7.9 mm ventral to the dura. The extent of
190 the dopamine lesion was assessed 14–16 days after 6-OHDA injection by challenge with apomorphine
191 (0.05 mg/kg, s.c.; Sigma) (Schwartz and Huston 1996b). The lesion was considered successful in
192 those animals that made >80 net contraversive rotations in 20 min. Electrophysiological recordings
193 were carried out ipsilateral to 6-OHDA lesions in anesthetized rats 21–42 days after surgery, when
194 pathophysiological changes in the basal ganglia are likely to have levelled out near their maxima
195 (Mallet et al. 2008a).

196 Data Acquisition and Analysis

197 Data Conversion and Pre-Processing

198 To isolate LFPs and ECoGs, all electrophysiological data were down-sampled from a hardware native
199 17.9 kHz to 250 Hz using Spike2 acquisition and analysis software (version 4; Cambridge Electronic
200 Design Ltd., Cambridge, UK). Data were then imported from Spike2 into MATLAB (The
201 Mathworks, Nantucket, MA, USA) where they were analysed using custom scripts utilizing routines
202 from the Fieldtrip software package (contained within SPM 12.3) (Oostenveld et al. 2011;
203 <http://www.fieldtriptoolbox.org/>), as well as Neurospec (<http://www.neurospec.org/>). Data were pre-
204 processed as follows: i) data were first truncated to remove 1 second from either end of the recording,
205 ii) mean subtracted; iii) band-passed filtered with a finite impulse response, two-pass (zero-lag) filter
206 designed such that the filter order is rounded to the number of samples for 3 periods of the lowest
207 frequency, between 4-100 Hz; iv) data were then split into 1 second epochs; v) each epoch was
208 subjected to a Z-score threshold criterion such that epochs containing any high amplitude artefacts
209 were removed. Examples of outcomes from this pre-processing are shown in figure 2. All ECoG/LFP
210 time series were 90-100 seconds in duration.

211 Analyses of Neurophysiological Signals

212 *Estimates of Spectral Power*

213 Power analyses were made using the averaged periodogram method across 1 second epochs and using
214 a Hanning taper to reduce the effects of spectral leakage. Frequencies between 49-51 Hz were
215 removed so that there was no contribution from 50 Hz line noise. The sampling rate of 250 Hz gives a
216 Nyquist frequency of 125 Hz and 1 second epochs yield Fourier spectra with a 1 Hz frequency
217 resolution and a periodogram resulting from an average of ~100 spectra per channel. All analyses
218 were made using the Neurospec toolbox. Individual spectra were normalized for group level
219 comparisons by dividing by the total power in the range 4-48 Hz.

220 *Non-zero Phase Lag Functional Connectivity Analysis: Imaginary Coherence*

221 The commonly used spectral coherence (Halliday et al. 1995) is sensitive to spurious correlations
222 resulting from instantaneous volume conduction between the two signals of interest (Bastos and
223 Schoffelen, 2016). This issue is of the most concern when recordings are made in close spatial
224 proximity such as that made by adjacent contacts on the silicon probes used in these experiments. In
225 order to circumvent this issue, several methods have been developed such as taking the imaginary part
226 of coherence (Nolte et al. 2004), the phase lag index (PLI) (Stam et al. 2007), or the weighted phase
227 lag index (Vinck et al. 2011). For this study, we used initially the simplest method - the imaginary
228 coherence (iCOH) that is derived from the complex coherency. The more often used coherence is the
229 magnitude-squared coherency. Coherence is real valued on a scale between 0-1, with 1 indicating
230 maximal correlation between two signals and 0 indicating an absence of correlation (Halliday et al.,

1995). Nolte and co-workers have suggested that by taking the imaginary part of the coherency, the contribution of correlations with zero phase lag (that is having only a real component) can be negated. This property is shared with the non-parametric directionality analysis that we will later introduce for estimates of directed connectivity. We note the concerns in Stam et al. (2007) on the validity of imaginary coherence analysis and so include additional analyses based on non-parametric directionality and use the iCOH metric as a first-pass demonstration that non-zero phase lag interactions are present in the data.

Non-Parametric Directionality

Estimates of directed connectivity were computed using non-parametric directionality (NPD) which is a novel framework to decompose classical, non-parametric Fourier-based, coherence estimates by direction (Halliday, 2015). Coherence between two random processes, or random signals, is defined as the ratio of the magnitude squared cross spectrum between the two signals to the product of their auto spectra. It is difficult to infer any directionality from this ratio involving cross spectra and auto-spectra. The approach introduced in Halliday (2015) uses optimal Minimum Mean Square Error (MMSE) pre-whitening of the two signals such that the coherence is calculated from the cross-spectrum only, as the denominator becomes equal to 1. Pre-whitening refers to the process of filtering a signal prior to spectral analysis to make its frequency content closer to white noise.

The pre-whitening step generates two new random processes which have spectra equal to 1 at all frequencies, and which have the same coherence as the two original signals. The coherence between the pre-whitened signals is calculated only from the cross spectrum between the pre-whitened processes and this is identical to the original coherence. From this MMSE pre-whitened cross spectrum an inverse Fourier transform generates a time domain correlation measure. This is analogous to the approach used to generate a standard cross-covariance estimate in the time domain, except the MMSE pre-whitened time domain correlation measure only has features that occur as a result of the correlation between the signals, effectively removing the confounding influence of the original signals' autocorrelation.

Three quantities are extracted from this time domain correlation measure according to time lag. These are components with negative time lags, the value at zero-time lag, and components at positive time lags. These are used to calculate the strength of correlation in the reverse, zero-lag and forward directions respectively. Three inverse Fourier transforms, using the sections over these three lags ranges, are used to obtain the reverse, zero-lag, and forward components of the original coherence estimate. These provide a summative decomposition of the original non-parametric coherence at each frequency into reverse, zero-lag and forward components.

In this study the zero-lag component is assumed to reflect volume conduction. The forward and reverse components of coherence are used to infer directionality between the different regions. For

266 example, STN activity lagging M2 activity results in a significant forward component of coherence
267 between M2 and STN (with M2 as reference), whereas STN activity leading M2 activity results in a
268 significant reverse component of coherence.

269 The concept of partial coherence is well established (Rosenberg et al., 1998; Medkour et al. 2009),
270 where coherence is conditioned on a third signal. This conditioning takes the form of a simple linear
271 regression in the frequency domain of each of the two original signals on the third signal or predictor.
272 The resulting partial coherence estimates can be used to test the hypothesis that the pairwise
273 correlation between the original signals can be accounted for by the third signal. The NPD framework
274 is extended to decompose partial coherence into directional components in Halliday et al (2016). The
275 analysis decomposes the partial coherence into the same three directional components: forward,
276 reverse and zero-lag. The approach is similar to the bivariate case, except MMSE pre-whitening is
277 applied using partial auto-spectra and the partial cross spectrum.

278 This analysis can indicate if the signals reflected in the correlation are common to other parts of the
279 network. For example, the partial correlation between A and B with C as predictor can be used to
280 determine if the flow of information from $A \rightarrow B$ is independent of area C, or whether the flow of
281 information is $A \rightarrow C \rightarrow B$, in which case the partial coherence between A and B with C as predictor
282 should be zero. The partial coherence can also be used to investigate if the flow of information is $C \rightarrow$
283 A and $C \rightarrow B$, or if it is $A \rightarrow B \rightarrow C$ or $C \rightarrow A \rightarrow B$, which for the latter case the partial coherence,
284 and any directional components should be zero.

285 This assumes that the conditioning signal, C, is representative of the activity in the relevant brain area.
286 If the signal, C, only captures part of the activity in the brain area then the partial coherence estimate
287 may still have residual features. The most robust interpretation of the partial coherence and
288 multivariate non-parametric directionality is where the partial coherence (and any directional
289 components) are not significant compared to the directional components for the ordinary coherence. It
290 must be noted that these methods are useful in detecting the linear coupling (additive mixing/linear
291 correlation) of signals. NPD is not suited for detection of non-linear interactions between signals such
292 as cross-frequency coupling for instance.

293 Statistics and Visualization

294 In order to make statistical comparisons of power, connectivity and directionality spectra between
295 lesioned and control recordings we used cluster based permutation testing (Maris and Oostenveld
296 2007) which avoids introducing bias through the prior specification of frequency bands. Briefly, the
297 method computes multiple independent t-statistics for each sample (channel-frequency pair) between
298 the two experimental conditions (lesion and control). We assume that in regions of the spectra where
299 there is a true physiological difference in the distributions of a metric of interest (i.e. power, iCOH,

300 NPD) there will be a high value of the t-statistic in several adjacent frequency bins and this group of
301 neighbouring bins is called ‘a cluster’.

302 The purpose of the cluster-based permutation test is to find clusters which are ‘heavier’ (i.e. have a
303 greater sum of t-statistic values in the cluster) than could be expected under the null hypothesis.
304 Candidate clusters to be tested are identified by setting a threshold on the t-statistic. Importantly, this
305 cluster-forming threshold does not affect the false alarm rate of the test, only the sensitivity to large
306 clusters with smaller t-values as opposed to small clusters with large t-values. The statistical
307 significance of candidate clusters is then tested by approximating the reference distribution using a
308 large number of permutations where the condition labels are randomly reassigned and the whole
309 procedure of cluster identification is repeated. The clusters in the original data are then compared to
310 the top tail of the reference distribution according to the pre-defined statistical threshold (typically,
311 5%). The permutation testing requires no assumption of normality and affords a correction for the
312 multiple comparison problem by controlling the family-wise error rate. For full details of the method,
313 see Maris (2012).

314 The cluster-forming threshold was $p < 0.05$ and the permutation test threshold was set at $p < 0.025$ (as it
315 is a two-sided test). The number of permutations was set to 5000 which tenders a lowest possible P-
316 value equal to 0.0004. Cluster statistics were computed using the ‘*ft_freqstatistics*’ routine in the
317 Fieldtrip toolbox. For testing of the effect of conditioning upon the NPD estimate, statistics are
318 computed identically as described above, but treating the conditioned and unconditioned spectra as
319 the two experimental conditions of interest. As each animal contained multiple recordings per
320 subcortical site we averaged the spectra from these recordings into a subject mean. Group level plots
321 indicate the group mean in bold ± 1 standard error of the mean (S.E.M.).

322 Results

323 Spectral Power

324 Examples of spectra computed from LFP and ECoG signals recorded in individual animals can be
325 seen in figure 2 (B and D). All the 6-OHDA-lesioned rats demonstrated a clear peak in the spectra in
326 the range 18-22 Hz (encompassing low beta/lower end of high beta frequencies) for LFP recordings
327 across all subcortical recording sites as well as for the sensorimotor ECoGs. In some animals, cortical
328 beta was weaker than that observed subcortically. None of the LFP data from control animals
329 contained beta peaks in the spectra although some (4 of 8) showed a wide, low amplitude peak around
330 20-40 Hz that was clearly above the $1/f$ background and most prominent in the recordings at M2 (an
331 example of which is seen in figure 2B). Analysis of the group averaged spectra (figure 3) shows that
332 the beta peak is significantly increased in the dopamine-depleted animals. Cluster-based permutation
333 testing demonstrated significant differences in group level spectra between control and lesion

334 conditions with clusters showing increases in power associated with dopamine depletion in the M2
335 (16-23 Hz, $P=0.001$), STR (18-21 Hz, $P=0.011$), STN (16-21 Hz, $P=0.012$), and GPe (17-22 Hz,
336 $P=0.008$). No differences between lesioned and control animals were found for frequencies >22 Hz in
337 any structures.

338 Functional Connectivity: Imaginary Coherence (iCOH)

339 Initial analyses of connectivity of the recorded LFPs using magnitude squared coherence showed
340 large magnitude (>0.9) wideband (0 - 60Hz) coherences that were indicative of a large field spread
341 effect (data not shown). This was most apparent in subcortical-subcortical analyses but was also
342 detected for cortical-subcortical pairings. To estimate coherence avoiding contamination by volume
343 conduction we opted to calculate non-zero phase lag correlations using the imaginary part of
344 coherence (iCOH) (see figure 4).

345 We found that activity in the low beta range (14-20 Hz) associated with 6-OHDA dopamine depletion
346 is spread diffusely across the network with all inter-regional comparisons showing a significant beta
347 peak in the iCOH spectrum. Notably, the strongest coherence in the low beta band involved STN,
348 with STN/STR and STN/GPe pairs both showing coefficients greater than 0.2. Within region
349 connectivity (i.e. STN contact 1 to contact 2) was found to be present in this frequency range for only
350 recordings within STN or GPe, where there is a clear beta peak. No within region connectivity was
351 found in the STR where the iCOH spectra were flat.

352 Analysis of statistical differences using the cluster based permutation testing between control and
353 lesioned animals showed significant increases of iCOH in the beta band in the lesioned animals and
354 for 5/10 LFP pairs tested: STN/STR (14-21 Hz, $P=0.006$), STN/STN (19-25 Hz, $P = 0.014$), GPe/STR
355 (14-16 Hz, $P = 0.010$), GPe/STN (14-21 Hz, $P=0.006$), and GPe/GPe (19-23 Hz, $P=0.004$). Notably,
356 no pairs involving M2 showed significant modulation of beta-band activity following dopamine
357 depletion when tested using cluster statistics. Taken generally, these results are indicative of
358 widespread, non-zero lag, low beta-band connectivity across the entire cortico-BG network that is
359 increased in the dopamine-depleted rats.

360 In the control rats, connectivity in the beta range was reduced relative to the dopamine depleted rats.
361 Instead, there was wide-band iCOH in the high beta/low gamma bands, ranging from 20 Hz to 50 Hz
362 in most cases but up to 70 Hz for the STN/M2 interactions. The majority of gamma band interactions
363 where iCOH was high (> 0.2) were found in connections involving the STN. Additionally, iCOH in
364 these bands is evident between GPe/M2 and GPe/STR although this was weaker (at around ~ 0.1) than
365 connections analysed with pairs involving the STN. iCOH in these bands is present in both the
366 lesioned and control animals and does not show a strong modulation by dopamine as evidenced by the
367 lack of significant clusters in the permutation tests for these bands. The iCOH analyses present
368 evidence for strong non-zero coherences at these frequencies even when spectral power at these

369 frequencies is small. It must be noted that there exists a separation between analyses of rhythmicity
370 and correlation of rhythmic activity that are complimentary properties of the signals.

371 Non-parametric Directionality (NPD)

372 We next investigated directed connectivity between recorded regions. The results of the analysis using
373 the NPD measure are presented in figure 5. The iCOH and the sum of the non-instantaneous parts
374 (forward and backward) of the NPD are similar, and both methods revealed similar patterns of
375 connectivity (data not shown). Analysis of the instantaneous (zero-lag) NPD in isolation demonstrated
376 the existence of high amplitude, wide-band interactions that were similar to those found with
377 magnitude squared coherence (data not shown), and are likely due to zero-phase field spread of
378 activity between recordings. Analyses of directional interactions of the LFPs and ECoG hereon will
379 use the forward and backward components of the NPD to discern directional connectivity between
380 LFPs recorded from each brain structure. Investigation of individual animals' functional connectivity
381 revealed that for the majority of animals the NPD spectra (and subsequently partialized spectra) were
382 well represented to that indicated by the group average.

383 We observed that directional interactions of low beta-band activity in the dopamine depleted animals
384 predominate in the direction leading from M2 and that they descend the hierarchy of the BG.
385 Interestingly we noted a significant difference in the cortical-subthalamic beta band interaction
386 between lesioned and control animals only in the feedback connection STN → M2 (16-18 Hz,
387 $P=0.020$), which would suggest that STN feedback to M2 is strengthened in the dopamine depleted
388 state. In the case of the STN/GPe circuit, and unlike iCOH, the non-instantaneous components of
389 NPD do not show 6-OHDA related increases in beta coupling in either direction for the lesioned rats.
390 Rather, NPD suggests a directional asymmetry in activity in the high beta/gamma band with forward
391 connections from GPe → STN connection stronger than in the reverse direction (cluster statistics
392 testing differences between forward and backward spectra in the 6-OHDA recordings: 4-43 Hz,
393 $P<0.001$). Notably, we see a feedback in the STN → STR that is most prominent in the lesion
394 condition, a feature that will be relevant with respect to results discussed later.

395 The pattern of activity in the high beta/gamma range between cortical and subcortical regions
396 appeared to be principally cortically leading with the coefficient of the interactions in the 20-40 Hz
397 range being up to 2/3 larger in the dopamine-intact control rats (top row of figure 5). Cluster-based
398 permutation analysis showed a significant increase in the high/gamma M2 → GPe NPD in the control
399 vs the lesion condition (25-30 Hz, $P=0.020$). High beta/gamma connections from subcortical
400 structures feeding back to M2, are weaker than the cortically leading connections, but are still present
401 for striatal and globus pallidus feedback to M2 (first column, row 2 and 4, figure 5). Again, there was
402 a clear peak in the high beta NPD from STN → STR in the lesioned animals, although a dependence
403 on dopamine was not seen to be significant when testing with cluster statistics. The finding of a large

404 NPD interaction from STN to STR does not accord with the canonical circuit (Figure 1A) but may
405 instead imply feedback to striatum via subcortical thalamo-striatal loops that will be discussed in a
406 later section of this paper.

407 **Inferring Routing of Brain Rhythms: Partialized Non-Parametric Directionality**

408 We repeated the NPD analysis as before but this time by systematically partialising out (conditioning)
409 the contribution made by LFPs/ECoG recorded from each brain structure to the bivariate analyses
410 presented in the previous section of the results. We again employed cluster statistics to determine
411 significant differences between the non-conditioned NPD spectra and its conditioned variant shown in
412 this section of the results.

413 **Conditioning the NPD using Local Field Potentials Recorded from the STN**

414 We first conducted a partialisation (conditioning) of the NPD estimate using LFPs recorded from
415 within the STN (figure 6). Conditioning with signals from the STN does not remove beta connectivity
416 between the remaining structures in the network although it does weaken the majority of comparisons
417 in the control (6 of 6 comparisons, red bars) but not the lesion (2 of 6 comparisons, blue bars) animals
418 (see figure 6, red and blue bars respectively). Cluster statistics indicate that the following NPDs for
419 the control experiments were significantly reduced by conditioning with the STN signal: M2 → STR
420 (14-33 Hz, $P < 0.001$), M2 → GPe (14-33 Hz, $P < 0.001$; 37-49 Hz, $P = 0.008$), STR → GPe (10-49 Hz,
421 $P < 0.001$), GPe → STR (18-49 Hz, $P < 0.001$) as well as feedback connections (returning to cortex):
422 STR → M2 (14-27 Hz, $P < 0.001$), GPe → M2 (18-49 Hz, $P < 0.001$). Furthermore, conditioning the
423 NPD with the signal from STN does not disrupt the 6-OHDA associated increases of M2 input to
424 either the STR (14-21 Hz, $P < 0.001$) or GPe (14-21 Hz, $P < 0.001$) (black bars). We also found in the
425 dopamine-depleted state that there was increased (relative to the controls) feedback to M2 from both
426 GPe (16-20 Hz, $P = 0.016$) and STR (16-20 Hz, $P = 0.006$).

427 Notably we observed some separation in the effects of the conditioning between the control and lesion
428 experiments. In the control animals conditioning the NPD on LFPs recorded at STN acted to reduce
429 activity in a wide band (~12-40 Hz) for the forward connections (propagating down the indirect
430 pathway; i.e. M2 → STR, M2 → GPe, and STR → GPe), whilst the return connections (STR → M2,
431 and GPe → M2) were only affected by conditioning at a tighter band corresponding to low beta. This
432 would suggest that in the healthy animal signals returning to cortex via STN occur at low beta
433 frequencies. Lesioned animals only showed reductions at higher frequencies (~24-45 Hz, high
434 beta/low gamma) and only between GPe and STR. We observed that conditioning of the NPD with
435 the STN signal acted to significantly reduce interactions between STR and GPe in both the forward
436 (STR → GPe, 23-49 Hz, $P < 0.001$) and reverse (GPe → STR, 27-49 Hz, $P = 0.001$) directions (red
437 bars).

438 Conditioning the NPD using Local Field Potentials Recorded from GPe

439 Next, we performed the NPD analysis of recorded signals but this time conditioning the interactions
440 with LFPs recorded from within the GPe (figure 7). We found that the conditioning had the effect of
441 reducing NPD estimates in 6 out of 6 possible connections in the controls and 3 out of 6 in the 6-
442 OHDA-lesioned rats. Most notably we found that the conditioning significantly attenuated (when
443 compared to the unconditioned NPD) the low beta band interaction in the M2 → STR connection for
444 both recordings made in control (red bar, 14-39 Hz, $P < 0.001$) and lesioned (blue bar, 14-21 Hz,
445 $P < 0.001$) animals implying that signals propagating through STR are highly correlated with that also
446 measured at GPe.

447 Secondly, we found a reduction of interactions between STR → STN across a wide range of
448 frequencies, again for both control (red bar, 6-49 Hz, $P < 0.001$) and lesioned (blue bar, 4-49 Hz,
449 $P < 0.001$) recordings suggesting signal routing is strongly mediated by GPe in accordance with the
450 canonical indirect pathway. Interestingly we found that although beta NPD in the M2 → STN
451 connection was attenuated by conditioning in the control recordings; for the 6-OHDA recordings, the
452 prominent low beta peak in the NPD remained and no significant effect of conditioning was observed.
453 Similarly, the STN → M2 feedback also retained a sharp beta peak that remained significantly
454 increased in recordings corresponding to the 6-OHDA lesion experiments (black bar, 14-20 Hz,
455 $P = 0.002$). Additionally, we found that when conditioning the STR → M2 NPD estimate with the GPe
456 signal there was an increased strength of interaction in the 6-OHDA treated animals (black bar, 16-21
457 Hz, $P < 0.001$).

458 In the high beta/gamma band we found that conditioning with GPe had a large effect in attenuating
459 the NPD in the forward connections (from M2 descending the indirect pathway) in the control
460 animals: M2 → STR (14-39 Hz, $P < 0.001$), M2 → STN (16-49 Hz, $P < 0.001$), and STR → STN (6-49
461 Hz, $P < 0.001$) (red bars). In the lesion animals only, 2 of the 6 comparisons made with NPD were
462 significantly attenuated in the 20-50 Hz range: STR → STN (4-49 Hz, $P < 0.001$) and STN → STR
463 (31-45 Hz, $P = 0.004$) (blue bars). This would imply that in control animals, high beta/gamma band
464 interactions in both directions between STN and STR are transmitted via (and linearly mixed with) a
465 signal at GPe.

466 Conditioning the NPD using Local Field Potentials Recorded from the STR

467 A third set of analyses used the local field potentials recorded at the STR to condition the NPD
468 estimates (figure 8). We found that this had the effect of destroying large parts of the descending
469 interactions (connections from M2 descending the hierarchy of the indirect pathway) in the control
470 animals, namely for M2 → GPe (16-37 Hz, $P < 0.001$) and M2 → STN (16-37 Hz, $P < 0.001$) (red bars).
471 In the lesion recordings, the effect of conditioning split into two ways: 1) Interactions between the
472 STN/GPe were significantly reduced across a very wide band ranging from low-beta to gamma

473 frequencies in both the STN → GPe (8-49 Hz, $P < 0.001$) and GPe → STN (6-49 Hz, $P < 0.001$)
474 coupling (blue bars) and 2) That interactions in the “hyper-direct” M2 → STN connection were not
475 attenuated, although note that the M2 → GPe (likely routed at least in part via the indirect pathway)
476 was suppressed by conditioning with the striatal signal (18-24 Hz, $P = 0.001$, blue bar). This peak is
477 also seen in the feedback connection from STN → M2 where the significant 6-OHDA associated
478 increase in beta feedback reported in previously analysis was found to remain (18-20 Hz, $P = 0.010$,
479 black bar).

480 Similar to the NPD estimates conditioned with signals recorded at GPe, we found that conditioning
481 with LFPs recorded at STR acted to largely remove the high beta/gamma interactions. In the M2 →
482 GPe connection in control animals we found that high beta/gamma activity was attenuated by STR
483 conditioning (16-37 Hz, $P < 0.001$); furthermore, we observed that 6-OHDA was associated with a
484 significant suppression of activity in this band (27-37 Hz, $P < 0.001$; 41-45 Hz, $P = 0.004$). Additionally,
485 we found that feedback in the high beta/gamma range (for control recordings) from GPe → M2 was
486 significantly attenuated by conditioning with the signal recorded at STR (14-41 Hz, $P < 0.001$, red bar).
487 Furthermore, this connection from GPe → M2, was significantly strengthened in the 6-OHDA
488 animals (35-41 Hz, $P = 0.002$, black bar).

489 Conditioning NPD Using Field Potentials Recorded from M2

490 The final analyses utilized ECoG signals recorded from the M2 to condition the BG NPD estimates
491 (results in figure 9). We found that the NPD estimates conditioned on M2 were generally flattened
492 and lacked distinct peaks at either low beta or high beta/gamma frequencies that were seen typically
493 in the other analyses. Altogether 5 of 6 NPD spectra had no distinct spectral peaks. When testing for
494 significant attenuation of NPD following conditioning we found that only control recordings were
495 significantly attenuated (4 of 6 connections, red bars), with high beta gamma peaks most clearly lost
496 in the STR → STN and STN → GPe interactions. The loss of features found in the unconditioned
497 NPD (such as beta or gamma peaks) were equivalent for both the control and 6-OHDA recordings.

498 When testing for the effects of 6-OHDA, we found that the STN → STR connection was significantly
499 altered. We observed a broad peak from 20-40 Hz in the lesion recordings that was not attenuated by
500 M2 conditioning and demonstrated a significant increase in strength associated with dopamine
501 depletion (21-27 Hz, $P = 0.007$, black bar).

502 Summary of Connectivity Analyses

503 Using recordings made in control and lesioned rats, we identified functional connectivity between
504 cortical and BG sites that involved either low beta or high beta/gamma oscillations. Broadly speaking,
505 we found that gamma connectivity is sensitive to the conditioning of structures upstream of the STN,
506 particularly GPe and STR, which removes gamma band oscillations from the spectra. In contrast, beta
507 connectivity was found to be robust to partializing using LFPs of any single BG structure. Cortico-

508 subthalamic connectivity in the beta range was unaffected by partialising of GPe or STR, suggesting
509 that M2/STN low beta connectivity is not routed via the indirect pathway. In the next section, we will
510 outline several putative models of oscillatory dynamics and present evidence from our analyses that
511 either support or weaken the plausibility of each model.

512 Discussion

513 Hypotheses and evaluation of evidence for signal propagation in the network

514 We have undertaken a systematic analysis of a dataset involving multisite ECoG/LFP recordings of
515 the cortico-basal ganglia circuit that contains data from a set of dopamine-intact control rats and
516 another set of rats with chronic dopamine depletion induced by a unilateral injection of 6-OHDA. We
517 will next discuss evidence for competing theories of the propagation of oscillatory activity across the
518 Parkinsonian cortico-basal ganglia circuit. We emphasise that our results are indicative of the
519 transmission of rhythmic activity in the circuit and cannot directly access the mechanisms that
520 generate these rhythms. However, as we will argue, results describing the patterns of synchronized
521 activity across the network and the changes that occur to them following dopamine depletion proffer
522 an important insight into how pathological rhythms differentially engage functional networks.

523 Mechanisms of the Flow of Beta Rhythms in the Basal Ganglia Circuit

524 Here we will evaluate the evidence provided by the analyses reported here in light of a number of
525 proposed theories concerning the generation and propagation of beta-band activity in the network and
526 the changes that occur during dopamine depletion that lead to its amplification. This work is
527 summarised in table 1.

528 *Hypothesis 1: Dopamine depletion in the basal ganglia induces increased beta resonance in the*
529 *cortical/STN “long-loop”.*

530 Previous authors have suggested that pathological beta rhythms are generated from the strengthening
531 of a long cortical feedback loop that returns from basal ganglia output nuclei via the thalamus.
532 Strengthened coupling is proposed to facilitate pathological resonance at beta frequencies (Brown
533 2007; van Albada and Robinson 2009; Dovzhenok and Rubchinsky 2012; Pavlides et al. 2015). The
534 first step towards verifying the plausibility of this hypothesis involves determining whether there is
535 indeed functional connectivity between STN and M2 in the beta band, and whether this occurs
536 independently of the cortico-striatal inputs to the indirect pathway.

537 Analysis of the iCOH for the M2/STN pairing suggests that functional connectivity in the beta band is
538 significantly strengthened in the lesioned animals compared to controls (figure 4). Analysis with NPD
539 demonstrates that there is a beta peak in the directed coherence in the low beta range in the forward
540 M2 → STN connection for both the control and 6-OHDA animals. Furthermore, in the lesioned
541 animals, the feedback connection (STN → M2) is significantly strengthened over that measured in the

542 controls. Neither the hyper-direct M2 → STN connection, nor the subthalamo-cortical feedback (STN
543 → M2) is diminished by either conditioning with signals from the GPe or STR in the lesioned animals
544 (figure 7 and figure 8). This suggests a reciprocal pathway between STN and M2 that is routed
545 independently of STR or GPe, most likely feeding back directly via the BG output nuclei. In contrast,
546 in control rats, NPD of the feedback connections at beta frequencies are significantly decreased by
547 conditioning with the STR signal in the forward (M2 → STN), and backward (STN → M2)
548 directions, suggesting that in the dopamine-intact anaesthetised state, beta band activity is routed via
549 STR, whilst the hyper-direct pathway is relatively quiescent. These findings support the idea that the
550 dopamine-depleted state is associated with a strengthening of the hyper-direct pathway and
551 subthalamo-cortical feedbacks.

552 Notably, this pathway is not active in isolation but coexists with beta propagation occurring along
553 striatal indirect pathway projections. Most notably, it was found that conditioning of the NPD with
554 LFPs recorded from the STN (figure 6) does not act to remove the 6-OHDA lesion associated beta
555 NPD in the structures ‘upstream’ of the STN (i.e. the STR and GPe). NPD in the low beta range is
556 significant in both directions along parts of the network involving either M2, STR or GPe. We find
557 that striatal-subthalamic interactions are strongly modulated by the GPe signal, a finding in line with
558 propagation down the canonical indirect pathway. Future work to validate the long-loop hypothesis
559 would involve the conditioning of the STN → M2 NPD using signals recorded from BG output nuclei
560 (either internal globus pallidus (GPi /EPN in rat) and/or SNr) or their major targets in the thalamus. If
561 these signals were available, then it would be possible better determine the routing of the cortical
562 return of BG beta activity from the STN.

563 *Hypothesis 2: Pathological beta is generated from strengthening of the reciprocally coupled*
564 *STN/GPe circuit.*

565 A separate hypothesis concerning the generation of pathological beta rhythms in the basal ganglia
566 considers the reciprocally coupled STN/GPe circuit from which increased coupling associated with
567 the loss of dopamine induces a pathological beta resonance that spreads across the rest of the network
568 (Plenz and Kital 1999; Bevan et al. 2002; Holgado et al. 2010; Tachibana et al. 2011).

569 We note that conditioning the NPD with the M2 signal does not remove the strong STN → GPe
570 directed connectivity, but it does attenuate the GPe → STN (figure 9). This indicates that activity
571 feeding back onto GPe from STN has a sufficiently unique temporal content so as not be partialized
572 out by the cortical ECoG, suggesting that pathological beta activity could be generated by some
573 resonance phenomenon arising from the tight, reciprocal coupling of STN and GPe. However, a
574 number of the analyses presented here suggest that pathological beta does not originate from an
575 autonomous STN/GPe resonator. These can be summarised as follows: 1) Comparison of forward
576 and backward NPD for STN/GPe interactions shows strong asymmetry, with the GPe → STN

577 connection predominating; 2) conditioning of the NPD using the LFPs recorded at the STR
578 significantly reduces the strength of both GPe \rightarrow STN and STN \rightarrow GPe NPDs in a way that appears
579 to be irrespective to dopaminergic state (figure 8), suggesting that beta activity in these structures
580 results from beta oscillations propagating through striatum; 3) conditioning the NPD with LFPs
581 recorded at the STN (figure 6) does not act to remove the upstream 6-OHDA associated beta NPD
582 between STR or GPe (although it does significantly weaken beta NPD in the control animals); 4) GPe
583 conditioned NPD analysis does not impair pathological M2/STN beta interactions (figure 7),
584 suggesting that the beta found at STN can be, at least in part, generated independently of a signal
585 found at GPe. The evidence given in point (1) may arise from the very tight coupling of the STN/GPe
586 pair, if full phase synchronization is occurring then the phase alignment between the two nuclei may
587 mislead the NPD to determine the phase leading population to be the drive, when in actuality there is
588 strong reciprocal coupling. The evidence in (2) and (3) points towards a mechanism of striatal
589 modulation of the STN/GPe circuit, perhaps via a pallidal-striatal feedback mechanism such as that
590 described by (Corbit et al. 2016). Taken together we argue these findings provide evidence against
591 pathological beta synchronization in the network arising from dissemination of an autonomously
592 generated rhythm in a STN/GPe “resonator”.

593 *Hypothesis 3: Beta arises through aberrant striatal activity and facilitation of downstream hyper-*
594 *synchrony.*

595 It has been proposed that aberrant striatal activity is involved in the emergence of pathological beta
596 rhythms in the BG arises due to changes to local dynamics within striatum (McCarthy et al. 2011;
597 Damodaran et al. 2015; Sharott et al. 2017); and/or a modification of striatal influence on the
598 STN/GPe sub-circuit (Terman et al. 2002; Kumar et al. 2011b; Sharott et al. 2017). From iCOH
599 analysis of signals recorded within striatum we do not find any local non-zero phase interactions
600 (unlike that which we find at STN). This finding would suggest that striatal-striatal transmission is
601 sparse, or phase aligned. Our results show that NPD measured at both the STN and GPe are
602 significantly weakened by conditioning with STR signals (figure 8) implying that striatal beta band
603 activity propagates down the indirect pathway. This would be in the line with the recent
604 demonstration that the firing of indirect pathway spiny projection neurons is aberrantly (and
605 selectively) entrained to exaggerated beta oscillations in lesioned rats (Sharott et al. 2017).

606 The weakening of NPD interactions from STR \rightarrow GPe and GPe \rightarrow STN when conditioning with M2
607 ECoG (figure 9), and only for the dopamine intact controls, may suggest that dopamine depletion
608 results in increased autonomy of the striatal (and indirect pathway) beta rhythm from beta at M2. In
609 support of this hypothesis, we also demonstrate that conditioning of the STR \rightarrow GPe NPD with the
610 STN signal is only effective (within the low beta range) in the control condition. This again
611 demonstrates that 6-OHDA lesioning results in a striatal signal that retains information independent
612 from that found at STN, providing evidence that it is likely the change of striatal output that occurs

613 following dopamine depletion. There is however some ambiguity as to whether the separation of the
614 striatal signal from that at the STN occurs due to changes to striatal dynamics or instead a change of
615 direct input to the STN such as from a strengthened hyperdirect input as discussed in hypothesis 1.

616 Hypotheses of the Origins/Routing of High Beta/Gamma Oscillations

617 The presence of high beta/gamma oscillations in the subcortical network has been noted by a number
618 of authors (Brown et al. 2002; Humphries et al. 2006; Berke 2009; Sharott et al. 2009; van der Meer
619 et al. 2010; Nicolás et al. 2011) but our understanding of the functional propagation of high
620 beta/gamma oscillations through the network is limited. An evaluation of the evidence we present in
621 this paper is summarised in table 2. We report gamma activity in the LFPs as well as connectivity in
622 the range 30-60 Hz which is in good agreement with that previously reported in anaesthetised rats
623 (Magill et al. 2004; Sharott et al. 2005b, 2009). Gamma activity in the awake and moving rat has also
624 been reported, albeit at slightly higher frequencies (Brown et al. 2002; Brazhnik et al. 2012; Delaville
625 et al. 2014).

626 *Hypothesis 4: High beta/gamma enters the subcortical network via the hyper-direct M2 → STN*
627 *connection.*

628 Results from analyses which used iCOH to investigate non-zero lag correlations between BG
629 structures and the cortex suggested that gamma interactions are routed in a way that bypasses STR as
630 a gamma peak is absent in the M2 (figure 4). This effect is most clear in the control recordings but
631 also to a lesser extent in the 6-OHDA experiments. The hyper-direct pathway is the other principal
632 source of cortical input to the BG, therefore the marked weakness of gamma interaction in the
633 M2/STR when compared to the M2/STN iCOH spectra may imply that the hyper-direct pathway is
634 responsible for gamma input to the network.

635 However, whilst there is a large peak in the high-beta/low-gamma band NPD for the M2 → STN
636 interaction (figure 5), if we examine the same connection but conditioned on LFPs either recorded at
637 STR (figure 7) or GPe (figure 8) we see that the conditioning significantly reduces NPD in the control
638 animals (M2 → STN conditioned on STR and M2 → STN conditioned on GPe), suggesting any
639 directed coherence between M2 and STN in these animals is routed via striatal-pallidal connections.
640 Furthermore, if we condition the NPD with LFPs recorded at the STN (figure 6), we see that gamma
641 interactions remain in the upstream components (M2 → STR, M2 → GPe) again suggesting striatal-
642 pallidal connectivity is vital in the propagation of gamma rhythms. When taken together, these data do
643 not supply strong evidence that the source of high beta/gamma input in the network is transferred by a
644 hyper-direct cortico-subthalamic route.

645 *Hypothesis 5: Gamma enters the network via cortico-striatal inputs and reaches STN via the indirect*
646 *pathway in a dopamine dependent manner.*

647 An alternative to high beta/gamma oscillations entering via hyper-direct STN input is that they are
648 channelled via the cortico-striatal indirect pathway. The clearest results of the NPD analysis in the
649 high beta/gamma band can be seen to be for the forward NPDs originating from M2 and passing on to
650 the subcortical regions (figure 5). Connections $M2 \rightarrow STR$, $M2 \rightarrow GPe$, and $M2 \rightarrow STN$ all show
651 high values of NPD in this frequency band (> 0.15) suggesting that most of the gamma is directed
652 from the cortex. Furthermore, conditioning the NPD with either LFPs recorded at the STR (figure 8)
653 or GPe LFPs (figure 7) acts to remove gamma interactions both upstream and downstream of the STR
654 (with respect to the indirect pathway). Subsequently, conditioning of the NPD with STN (figure 6) is
655 less effective at attenuating gamma band interactions than when using signals higher in the indirect
656 pathway, suggesting that the gamma descends the hierarchy, from either a cortical or striatal source.
657 Notably, we observed that STN conditioned NPD did not act to attenuate feedback connections from
658 GPe or STR back to the M2. This would suggest routing of gamma to the M2 in a way that occurs
659 independently of STN.

660 In attempt to elucidate the source of the gamma activity we conditioned the NPD on the cortical
661 ECoG (figure 9). We find that gamma connectivity in the control recordings and in dopamine
662 depletion states acts to significantly reduce NPD coefficients for the $GPe \rightarrow STN$ and $STR \rightarrow STN$
663 connections, yet the feedback connection $STN \rightarrow STR$ is unaffected. This connection in the control
664 animals shows a peak from 18-42 Hz which is significantly larger than in the lesioned animals. This is
665 in agreement with the hypothesis that gamma rhythms are pro-kinetic; this idea is also supported by
666 patients' data (Sharott et al. 2014). Furthermore, these findings suggest that gamma activity is directed
667 to upstream components of the indirect pathway in a way independent of M2, perhaps mediated via a
668 subcortical feedback loop.

669 *Hypothesis 6: High beta/gamma is generated locally within the basal ganglia network either at STR,*
670 *STN or GPe*

671 The finding that conditioning the NPD with cortical ECoG does not entirely abolish gamma
672 connectivity within the BG suggests a possible subcortical high beta/gamma generator, or
673 alternatively a source in the cortex that has not been measured in our experiments. Work by
674 Kondabolu et al. (2016) has demonstrated that the optogenetic activation of striatal cholinergic
675 interneurons is sufficient to generate gamma rhythms locally, although not in a way clearly separable
676 from low frequency beta. However, when applying iCOH to signals recorded within STR we find no
677 evidence for local interactions in the high beta/gamma band. Simulations of the BG spiking network
678 by Humphries et al. (2006) suggest that upper-gamma band (40-80 Hz) activity can arise as a result of
679 coupling between the STN and GPe. When we conditioned the NPD with LFPs recorded from either
680 the GPe (figure 7) or STR (figure 8), we found that interactions in the high beta/gamma frequency

681 ranges were abolished in the majority of other subcortical interactions. This would imply that these
682 GPe and STR structures are necessary for the propagation of high beta/gamma interactions in the both
683 the control and 6-OHDA lesion animals. This in combination with the evidence provided for
684 hypothesis 5 suggests that high beta/gamma can originate at either STR or GPe and then propagate to
685 downstream structures. Backward gamma interactions from GPe to STR are apparent in the NPD
686 conditioned on either M2 or STN, suggesting the STR signal is the result of local propagation of a
687 gamma signal from GPe. From the canonical circuit perspective it is not clear how gamma passes
688 upstream from GPe. However, a substantial proportion of GPe neurons that innervate the striatum
689 have been shown to exist, with one GPe cell type (arkypallidal neurons) projecting exclusively to
690 striatum (Mallet et al. 2012; Abdi et al. 2015; Hegeman et al. 2016). This same pathway has been
691 proposed by Corbit et al. (2016) to promote synchronization in the low beta range but the same
692 arguments are likely to apply to high beta/low gamma frequencies.

693 Summary of Findings

694 In this paper, we have investigated the propagation of oscillatory activity through connected regions
695 of the cortico-basal ganglia network. We have applied a novel model-free method of partialized
696 directed connectivity to achieve a systematic deconstruction of the propagation of rhythmic activity
697 between regions of the network inferred from the LFPs and ECoGs recorded at multiple sites within
698 that network. Using the 6-OHDA-lesioned rat model of Parkinsonism, we demonstrate marked
699 differences in the patterns functional connectivity that result as a consequence of dopamine depletion
700 in the BG.

701 We find widespread beta synchronization of LFPs across the network that is strongly associated with
702 chronic dopamine depletion. With regards to functional beta connectivity in the network we find
703 evidence for:

- 704 1. An increased cortical entrainment of the basal ganglia following dopamine depletion.
- 705 2. Significant beta-band connectivity between structures interacting with the STN that is
706 independent of activity upstream in the indirect pathway (at STR and GPe). This is likely to
707 originate from the ‘hyperdirect’ cortico-subthalamic input.
- 708 3. Increase in feedback of BG structures to M2 after dopamine depletion, proffering evidence in
709 favour of a hypothesis of dopamine-dependent modulation of the long re-entrant cortico-BG-
710 thalamo-cortical loop.
- 711 4. Activity dynamics of the STN/GPe sub circuit that are partly dependent upon output from
712 striatum.
- 713 5. A feedback from STN to STR that is independent of M2 and significantly strengthened after
714 dopamine depletion, suggesting a strengthening of recurrent subcortical circuits.

715 Furthermore, we provide evidence for the existence of high beta/gamma synchrony within the
716 network, with evidence that dopamine depletion acts to weaken these rhythms. We summarise our
717 findings with respect to high beta/gamma band interactions in the following:

- 718 1. Gamma propagates down the indirect pathway from STR to GPe to STN. This activity is
719 likely to be generated at the level of the cerebral cortex.
- 720 2. Evidence of gamma activity found at STN that is independent of M2 and evidence for a
721 subcortical return of subthalamic outputs back to striatum.
- 722 3. Evidence for gamma activity returning to the cortex that is independent of STN, perhaps
723 indicating propagation through the direct pathway.

724 Propagation of Low Beta via two Coexisting but Distinct Streams

725 In the case of low beta oscillations, we find our data most strongly support a hypothesis that in the
726 dopamine-depleted condition, beta propagation in the network is biased to favour low beta synchrony
727 via induction of a long cortico-subthalamic loop that inputs to the BG via the hyper-direct pathway.
728 Furthermore, we see evidence that the return connection from STN to M2 is significantly stronger in
729 the lesioned animals when compared to dopamine-intact controls. This provides supporting evidence
730 for the notion that pathological beta amplification arises from entrainment of the re-entrant
731 cortical/STN loop (Brittain and Brown 2014). We speculate that strengthening of the hyper-direct
732 input acts to “short-circuit” the network, such that transmission of information along the indirect
733 pathway is compromised. Oswal et al. (2016) have provided evidence that deep brain stimulation in
734 patients acts to selectively suppress activity mediated synchrony between mesial premotor regions and
735 the STN which is proposed to be mediated by the hyper-direct pathway. In the “hold your horses”
736 model of the STN’s role in decision making (Frank 2006; Frank et al. 2007), the hyper-direct pathway
737 is proposed to provide a cortical veto signal which may act to suppress premature action. In the case
738 of PD, over activity of this circuit via increased resonance may act to lock the network into a state that
739 ultimately suppresses action and movement. These findings are in agreement with previous research
740 which have found good evidence for bidirectional connectivity between STN and cortex (Lalo et al.
741 2008; Jávora-Duray et al. 2015).

742 This hypothesis requires further testing through analysis of the role of the BG output nuclei at GPi or
743 SNr (or their targets in the thalamus) in the propagation of activity. This could be achieved using a
744 functional ‘lesion’ approach like that described in this paper. Furthermore, biophysical modelling of
745 the cortico-subthalamic loop may yield insight as to whether this is a plausible mechanism given the
746 known conduction delays for the connections in the network. Long feedback loops involving cortex
747 have been demonstrated to be capable of generating oscillatory activity (Leblois et al. 2006; Pavlides
748 et al. 2015). Work by Shouno et al. (2017) suggests that the required delay for the return of the beta
749 oscillation from STN to cortex may be too great to support resonance in the low beta band and

750 possibly the engagement of shorter subcortical loops either subcortical-thalamic loops (McHaffie et
751 al. 2005) or activity of recurrent subthalamo-striatal projections (Sato et al. 2000; Koshimizu et al.
752 2013) may be more suitable candidates for supporting beta oscillations through resonance.

753 The analysis presented here also suggests that a cortico-subthalamic pathway is not the exclusive
754 pathway for beta rhythms within the network, yet may be necessary for enhancement of the STN
755 feedback to cortex that may induce pathological resonance. We would suggest that both the
756 hyperdirect and indirect routes for beta propagation coexist. These two pathways could originate from
757 and be driven by, distinct populations of cortical projections neurons (namely those of the pyramidal
758 tract and intra-telencephalic projections, respectively) and so are likely to show a degree of
759 independence from one another. The data presented here also suggest a second pathway upstream of
760 STN involving the STR that is most evident in the recordings from control rats. We suggest that both
761 pathways contain signals shared by activity measured in the cortical ECoG: conditioning of the NPD
762 acts to remove beta peaks from the majority of connections that were analysed, leaving just beta
763 coherence at the STR → STN connection. These findings support the hypothesis that dopamine cell
764 loss acts to increase the sensitivity of the STR to cortical inflow, disrupting the striatum's role in
765 gating activity to the remainder of the circuit (Magill et al. 2001; Tseng et al. 2001; Sharott et al.
766 2017).

767 Notably, our data do not support the hypothesis of beta generation via an autonomous STN/GPe
768 pacemaker network, as directional coherence between the two is heavily attenuated by conditioning
769 with LFPs recorded upstream in the STR and there is significant asymmetry in the NPD with the
770 globus pallidus drive predominating. In agreement, Moran et al. (2011) found evidence for a
771 weakening of the STN to GPe feedback connection in the dopamine depleted state, conflicting with
772 the STN/GPe resonance hypothesis. It may be the case that tight coupling of the STN and GPe results
773 in a near fixed phase relationship in which there is reciprocal coupling yet from the perspective of
774 phase, the GPe appears to lead.

775 Estimates of effective connectivity from DCM studies have also suggested that input from cortex to
776 STN is strengthened in the Parkinsonian state (Moran et al. 2011), a finding consistent with the idea
777 that dopamine enforces cortical influence upon the STN/GPe network (Magill et al. 2001; Leblois
778 2006; Leblois et al. 2006; Holgado et al. 2010). It is possible that in PD, cortical activity subsumes the
779 STR as the primary driver of the STN/GPe sub-circuit, effectively acting to “short-circuit” the system.
780 It has been demonstrated that movement is associated with a decreased cortico-pallidal coherence
781 during movement in humans (van Wijk et al. 2017) suggesting that disengagement of cortical
782 influence via this pathway is pro-kinetic. Thus pathological resonance may arise following dopamine
783 depletion through a compensatory mechanism of increased hyperdirect input following an altered or
784 reduced striatal output (Kumar et al. 2011a; Damodaran et al. 2015). In the healthy system it has been

785 proposed that this works to actively de-correlate spiking activity between the two structures (Wilson
786 2013). The action of dopamine upon these inputs is likely to lead to the promotion of beta amplifying
787 phase alignments between STN and GPe such as that observed by Cagnan, Duff, & Brown (2015).

788 Dopamine Depletion is Associated with an Increased Subthalamo-Striatal Feedback

789 Taken together, the analyses presented here speak to the existence of a high beta/low gamma rhythm
790 that is in general reduced by dopamine depletion. Specifically, our results indicate that connectivity in
791 the frequency band 27-34 Hz is attenuated by the 6-OHDA lesion. Experiments investigating LFPs in
792 the motor cortex of moving rats have demonstrated an increase in activity in this band during
793 movement suggesting that activity at these frequencies in M2 and SNr is pro-kinetic (Brazhnik et al.
794 2012). Our data would suggest that high beta/gamma activity in the normal network is predominantly
795 entrained by the cortex as evidenced by: 1) the unconditioned NPD indicates that gamma is
796 prominently in the forward direction leading from cortex to subcortical sources; and 2) conditioning
797 the NPD on ECoG recorded at M2 acts to diminish the subcortical directional coherence across a wide
798 band for all connections not involving STN. However, evidence by Zold and colleagues has
799 demonstrated that oscillatory activity >20 Hz in corticostriatal afferents is not effectively transmitted
800 through the striatum (Zold et al. 2012) suggesting that the actual mechanism is likely to be more
801 complicated.

802 Furthermore, following partialization some interactions involving STN do remain. In particular we
803 provide evidence for a significant strengthening of feedback from STN to STR in the lesioned animals
804 in the high beta/gamma band. We speculate that this signal is facilitated through the strengthening of
805 subcortical loops such as that of the thalamo-striatal pathways (McHaffie et al. 2005). Thalamic
806 afferents make up to at least 25% of input onto spiny projection neurons in the STR (Doig et al. 2010;
807 Smith et al. 2014) but have been far less studied than cortical inputs. Work investigating synaptic
808 remodelling following 6-OHDA depletion in mice has suggested that thalamo-striatal inputs to
809 medium spiny neurons are shifted in favour of the indirect pathway (Parker et al. 2016) perhaps
810 enhancing striatal return of subthalamic activity in a mechanism independent of cortex.

811 Segregation of Low Beta and High Beta/Gamma Functional Networks

812 Our analyses present a clear separation in the patterns of inter-areal synchronization between low beta
813 and high beta/low gamma frequencies. We find pathological low beta correlations to be present across
814 large parts of the network, and resistant to conditioning with signals from connected structures. In
815 contrast, high beta/gamma shows a much more hierarchical organization, descending the indirect
816 pathway and possibly looping back subcortically through subthalamic-striatal feedback. Furthermore,
817 high beta/gamma correlations appear to be weakened by the 6-OHDA lesion.

818 Multiple studies investigating the electrophysiology of patients with PD (Priori et al. 2004; López-
819 Azcárate et al. 2010) have found evidence for the functional differentiation between low and high beta

820 frequency activity. Low beta is found to be increased by dopamine depletion and correlates with
821 bradykinetic/rigid symptoms in patients, whereas high beta is less responsive to dopamine changes.
822 Interestingly, dopamine replacement in patients has been shown to decouple high and low beta
823 frequencies when analysing with spectral bicoherence (Marceglia et al. 2006). Cortico-subthalamic
824 coherence is also found at this frequency in patients, although again this is largely unresponsive to
825 dopamine (Litvak et al. 2011b). We also find evidence for high beta coherence between BG and
826 cortex although unlike that found in patients, we find this connectivity to be weakened and shifted to
827 low beta frequencies by 6-OHDA induced dopamine depletion.

828 In the current paper we have not made analysis of the interaction or co-existence of the two frequency
829 bands described. This is an interesting problem as the beta network is more responsive to dopamine
830 depletion than that at the high beta/gamma frequencies. Future work may utilise tools such as
831 analysis of cross-frequency coupling and time resolved spectral analysis to do so.

832 Study Limitations

833 Incomplete Signals for Conditioning

834 The use of partial coherence for inferring neural connectivity is not in itself a novel approach
835 (Rosenberg et al. 1998; Eichler et al. 2003; Salvador et al. 2005; Medkour et al. 2009), and the
836 application of the partialized NPD to LFPs recorded in the rat hippocampus has been previously
837 reported (Halliday et al. 2016). However, these analyses assume that the signals used for conditioning
838 completely capture the activity going through the proposed pathway. This however is unlikely to be
839 entirely the case due to the finite sampling of the structures afforded from the use of electrodes. That
840 said the large number of channels used for recordings in the present study ensure that multiple
841 samples are obtained from within each brain structure. In the data presented here, subcortical
842 structures were recorded from between 2-8 different channels which were all used to condition the
843 estimate of directed coherence. It should also be noted that this sampling limitation is likely to apply
844 most to the larger structures that were analysed, namely the motor cortex and striatum, whereas
845 recordings from the smaller sized STN are more likely to capture a larger share of the total activity.
846 This factor must be considered when interpreting conditioning of the NPD with respect to STR
847 signals. It could be the case that M2 → STN connectivity remains in the face of conditioning with the
848 STR LFP as a result of incomplete sampling of neural fields within striatum.

849 Inference of Connectivity from Non-Spiking Brain Activity

850 This study is based upon an analysis of mesoscale recordings of brain activity as measured either in
851 the ECoG or the LFP. Transmission of information in the brain is due to axonal propagation of action
852 potentials is not explicitly captured in these signals. LFPs and ECoG comprise a conglomerate of sub-
853 and supra- threshold events that may or may not be tied to spike activity and so direct inference of
854 neurophysiological connectivity *per se* is limited by this. Nonetheless, spike timing has been shown to

855 tightly correlate with negative deflection of the LFP (Destexhe et al. 1999) and increasing evidence
856 that the field itself modulates neural activity is emerging (Qiu et al. 2015; Goldwyn and Rinzel 2016).
857 With respect to the basal ganglia, it has been previously demonstrated by Mallet and colleagues that
858 beta-band activity in the LFPs recorded at STN and GPe of lesioned rats are associated with increased
859 bet-frequency synchronization of action potential firing by neurons in these structures (Mallet et al.
860 2008a, 2008b) but see also Magill et al. (2004) where coupling of GPe units and slow wave activity in
861 the LFP is relatively weak in dopamine-intact rats. Furthermore, we provide evidence for the
862 existence of temporally lagged correlations between rhythmic local field potentials recorded between
863 distinct regions of the cortico-BG network that imply causation from one signal to another, a
864 phenomenon that would itself not be possible without the transmission of action potentials. Future
865 work will require an investigation to determine whether directional interactions are ascertainable from
866 multiunit activity and how this relates to lagged synchronization of LFPs.

867 Limits to Inference of Causal Interactions and Mechanisms from Neurophysiological Signals 868 Alone

869 In this paper, we aim to infer how neural activity propagates across the BG network by investigating
870 the statistical relationships between brain signals. The challenges that this approach face are well
871 documented (Friston 2011; Bastos and Schoffelen 2016). With respect to this study, the benefits that
872 that we claim for using a model free, non-parametric approach (namely agnosticism to the underlying
873 generating mechanisms of the data) may in turn limit the degree of inference that can be made.
874 Estimates of directed functional connectivity in this paper follow from the assumptions that temporal
875 precedence is indicative of causation. It is however well documented that zero lag synchronization can
876 emerge from neural circuits with particular (but not unusual) network motifs (Vicente et al. 2008;
877 Viriyopase et al. 2012; Gollo et al. 2014). Additionally, “anticipatory” synchronization in which
878 positive lags arise from a directed input have also been described in theoretical neural dynamics
879 (Ambika and Amritkar 2009; Ghosh and Roy Chowdhury 2010; Matias et al. 2011). The anatomically
880 tightly coupled STN-GPe sub-circuit is a prime candidate for which these phenomena may permit
881 vanishingly small phase lags that make the interactions blind to NPD. Answers to these problems may
882 be given in the future by the fitting of biophysical models to the data presented in this paper. This
883 would provide a well-defined, quantitative description of the potential mechanisms that act to
884 generate the phenomena we have described.

885 Furthermore, this study makes inference from the sample statistics of the experimental groups and
886 does not make systematic investigation as to the existence of heterogeneity in the functional
887 connectivity of the group. Such work would likely involve cluster analysis of the connectivity in order
888 to ask the interesting question of whether localized dopamine depletion can result in a range of
889 distinct individual patterns of beta/gamma propagation.

890 Moreover, we must stress that analysis of functional connectivity cannot access directly the
891 mechanisms that generate sustained neural oscillations and their synchronization. This requires direct
892 experimental manipulations of connections in the network such as that by Tachibana et al. (2011).
893 Nonetheless, the biophysical transmission of rhythmic neural activity and the changes that occur to it
894 following a manipulation such as the 6-OHDA induced ablation of dopamine neurons leave behind a
895 signature that is accessible to the tools of functional connectivity. Further, the ability to apply
896 systematic “functional lesions” such as that afforded by the conditioned NPD analysis, only acts to
897 more increase our ability to infer the generative mechanisms of the observed data.

898 Conclusion

899 Overall, we provide a systematic deconstruction of the propagation of pathological rhythms across the
900 Parkinsonian cortico-basal ganglia circuit *in vivo*. These findings strengthen our understanding of how
901 normal and pathological rhythms propagate across the network. Our work highlights the importance
902 of considering non-canonical connections in the network, in particular the activity of recurrent
903 subcortical projections that may act to amplify pathological activity within the BG. Future work will
904 aim to understand the exact changes to the network required to generate the patterns of functional
905 connectivity presented here, as well as to investigate the relationship with spiking activity in the
906 network.

907 Acknowledgments

908 We thank Dr N. Mallet for acquiring some of the primary data sets. T.O.W. thanks UCL CoMPLEX
909 for their continued funding and support.

910 Funding

911 Medical Research Council UK (awards UU138197109, MC_UU_12020/5 and MC_UU_12024/2 to
912 P.J.M.; MC_UU_21024/1 to A.S.). Parkinson’s UK (Grant G-0806 to P.J.M.). S.F.F. receives funding
913 from UCLH BRC. Engineering Research Council UK (awards EPSRC EP/F500351/1 to T.O.W.;
914 EP/N007050/1 to D.H.). The Wellcome Trust Centre for Neuroimaging is funded by core funding
915 from the Wellcome Trust (539208).

916 References

- 917 **Abdi A, Mallet N, Mohamed FY, Sharott A, Dodson PD, Nakamura KC, Suri S, Avery S V,**
918 **Larvin JT, Garas FN, Garas SN, Vinciati F, Morin S, Bezard E, Baufreton J, Magill PJ.**
919 Prototypic and arky pallidal neurons in the dopamine-intact external globus pallidus. *J Neurosci* 35:
920 6667–88, 2015.
- 921 **van Albada SJ, Robinson PA.** Mean-field modeling of the basal ganglia-thalamocortical system. I:
922 Firing rates in healthy and parkinsonian states. *J Theor Biol* 257: 642–663, 2009.

- 923 **Ambika G, Amritkar RE.** Anticipatory synchronization with variable time delay and reset. *Phys Rev*
924 *E* 79: 56206, 2009.
- 925 **Bastos AM, Schoffelen J-M.** A Tutorial Review of Functional Connectivity Analysis Methods and
926 Their Interpretational Pitfalls. *Front Syst Neurosci* 9: 175, 2016.
- 927 **Berke JD.** Fast oscillations in cortical-striatal networks switch frequency following rewarding events
928 and stimulant drugs. *Eur J Neurosci* 30: 848–859, 2009.
- 929 **Beudel M, Oswal A, Jha A, Foltynie T, Zrinzo L, Hariz M, Limousin P, Litvak V.** Oscillatory
930 Beta Power Correlates With Akinesia-Rigidity in the Parkinsonian Subthalamic Nucleus. *Mov Disord*
931 32: 174–175, 2017.
- 932 **Bevan MD, Magill PJ, Terman D, Bolam JP, Wilson CJ.** Move to the rhythm: oscillations in the
933 subthalamic nucleus–external globus pallidus network. *Trends Neurosci* 25: 525–531, 2002.
- 934 **Bolam JP, Hanley JJ, Booth PA, Bevan MD.** Synaptic organisation of the basal ganglia. *J Anat* :
935 527–42, 2000.
- 936 **Brazhnik E, Cruz A V., Avila I, Wahba MI, Novikov N, Ilieva NM, McCoy AJ, Gerber C,**
937 **Walters JR.** State-Dependent Spike and Local Field Synchronization between Motor Cortex and
938 Substantia Nigra in Hemiparkinsonian Rats [Online]. *J Neurosci* 32, 2012.
939 <http://www.jneurosci.org/content/32/23/7869.long> [2 May 2017].
- 940 **Bressler SL, Menon V.** Large-scale brain networks in cognition: emerging methods and principles.
941 *Trends Cogn Sci* 14: 277–290, 2010.
- 942 **Brittain J-S, Brown P.** Oscillations and the basal ganglia: motor control and beyond. *Neuroimage*
943 85: 637–647, 2014.
- 944 **Brown P.** Abnormal oscillatory synchronisation in the motor system leads to impaired movement.
945 *Curr Opin Neurobiol* 17: 656–664, 2007.
- 946 **Brown P, Kupsch A, Magill PJ, Sharott A, Harnack D, Meissner W.** Oscillatory Local Field
947 Potentials Recorded from the Subthalamic Nucleus of the Alert Rat. 2002.
- 948 **Brown P, Oliviero A, Mazzone P, Insola A, Tonali P, Di Lazzaro V.** Dopamine Dependency of
949 Oscillations between Subthalamic Nucleus and Pallidum in Parkinson’s Disease [Online]. *J Neurosci*
950 21: 1033–1038, 2001. <http://www.jneurosci.org/content/21/3/1033.abstract> [4 Jan. 2016].
- 951 **Cagnan H, Duff EP, Brown P.** The relative phases of basal ganglia activities dynamically shape
952 effective connectivity in Parkinson’s disease. *Brain* 138: 1667–1678, 2015.
- 953 **Corbit VL, Whalen TC, Zitelli KT, Crilly SY, Rubin JE, Gittis AH.** Pallidostriatal Projections

- 954 Promote β Oscillations in a Dopamine-Depleted Biophysical Network Model. *J Neurosci* 36: 5556–
955 71, 2016.
- 956 **Damodaran S, Cressman JR, Jedrzejewski-Szmek Z, Blackwell KT.** Desynchronization of Fast-
957 Spiking Interneurons Reduces β -Band Oscillations and Imbalance in Firing in the Dopamine-Depleted
958 Striatum [Online]. *J Neurosci* 35, 2015. <http://www.jneurosci.org/content/35/3/1149.long> [19 Jul.
959 2017].
- 960 **Deco G, Jirsa VK, Robinson PA, Breakspear M, Friston K.** The dynamic brain: from spiking
961 neurons to neural masses and cortical fields. *PLoS Comput Biol* 4: e1000092, 2008.
- 962 **Deco G, Senden M, Jirsa V.** How anatomy shapes dynamics: a semi-analytical study of the brain at
963 rest by a simple spin model. *Front Comput Neurosci* 6: 68, 2012.
- 964 **Delaville C, Cruz A V, McCoy AJ, Brazhnik E, Avila I, Novikov N, Walters JR.** Oscillatory
965 Activity in Basal Ganglia and Motor Cortex in an Awake Behaving Rodent Model of Parkinson's
966 Disease. *Basal Ganglia* 3: 221–227, 2014.
- 967 **DeLong M, Wichmann T.** Changing views of basal ganglia circuits and circuit disorders. *Clin EEG*
968 *Neurosci* 41: 61–7, 2010.
- 969 **Destexhe A, Contreras D, Steriade M.** Spatiotemporal Analysis of Local Field Potentials and Unit
970 Discharges in Cat Cerebral Cortex during Natural Wake and Sleep States [Online]. *J Neurosci* 19:
971 4595 LP-4608, 1999. <http://www.jneurosci.org/content/19/11/4595.abstract>.
- 972 **Doig NM, Moss J, Bolam JP.** Cortical and Thalamic Innervation of Direct and Indirect Pathway
973 Medium-Sized Spiny Neurons in Mouse Striatum [Online]. *J Neurosci* 30, 2010.
974 <http://www.jneurosci.org.libproxy.ucl.ac.uk/content/30/44/14610> [24 Aug. 2017].
- 975 **Donoghue JP, Wise SP.** The motor cortex of the rat: Cytoarchitecture and microstimulation mapping.
976 *J Comp Neurol* 212: 76–88, 1982.
- 977 **Dostrovsky J, Bergman H.** Oscillatory activity in the basal ganglia--relationship to normal
978 physiology and pathophysiology. *Brain* 127: 721–722, 2004.
- 979 **Dovzhenok A, Rubchinsky LL.** On the Origin of Tremor in Parkinson's Disease. *PLoS One* 7, 2012.
- 980 **Eichler M, Dahlhaus R, Sandkuhler J.** Partial correlation analysis for the identification of synaptic
981 connections. *Biol Cybern* 89: 289–302, 2003.
- 982 **Eusebio a, Thevathasan W, Doyle Gaynor L, Pogosyan a, Bye E, Foltynie T, Zrinzo L, Ashkan**
983 **K, Aziz T, Brown P.** Deep brain stimulation can suppress pathological synchronisation in
984 parkinsonian patients. *J Neurol Neurosurg Psychiatry* 82: 569–573, 2011.

- 985 **Frank MJ.** Hold your horses: A dynamic computational role for the subthalamic nucleus in decision
986 making. *Neural Networks* 19: 1120–1136, 2006.
- 987 **Frank MJ, Samanta J, Moustafa AA, Sherman SJ.** Hold your horses: impulsivity, deep brain
988 stimulation, and medication in parkinsonism. *Science* 318: 1309–12, 2007.
- 989 **Fries P.** A mechanism for cognitive dynamics: neuronal communication through neuronal coherence.
990 *Trends Cogn Sci* 9: 474–480, 2005.
- 991 **Fries P.** Rhythms for Cognition: Communication through Coherence. *Neuron* 88: 220–235, 2015.
- 992 **Friston KJ.** Functional and Effective Connectivity: A Review. *Brain Connect* 1: 13–36, 2011.
- 993 **Ghosh D, Roy Chowdhury A.** Lag and anticipatory synchronization based parameter estimation
994 scheme in modulated time-delayed systems. *Nonlinear Anal Real World Appl* 11: 3059–3065, 2010.
- 995 **Gillies A, Willshaw D.** Models of the subthalamic nucleus: The importance of intranuclear
996 connectivity. *Med Eng Phys* 26: 723–732, 2004.
- 997 **Goldwyn JH, Rinzel J.** Neuronal coupling by endogenous electric fields: cable theory and
998 applications to coincidence detector neurons in the auditory brain stem. *J Neurophysiol* 115: 2033–51,
999 2016.
- 1000 **Gollo LL, Mirasso C, Sporns O, Breakspear M.** Mechanisms of Zero-Lag Synchronization in
1001 Cortical Motifs. *PLoS Comput Biol* 10: e1003548, 2014.
- 1002 **Halliday D, Rosenberg JR, Amjad A, Breeze P, Conway BA, Farmer SF.** A framework for the
1003 analysis of mixed time series/point process data—Theory and application to the study of physiological
1004 tremor, single motor unit discharges and electromyograms. *Prog Biophys Mol Biol* 64: 237–278,
1005 1995.
- 1006 **Halliday DM, Senik MH, Stevenson CW, Mason R.** Non-parametric directionality analysis –
1007 Extension for removal of a single common predictor and application to time series. *J Neurosci*
1008 *Methods* 268: 87–97, 2016.
- 1009 **Hammond C, Bergman H, Brown P.** Pathological synchronization in Parkinson’s disease: networks,
1010 models and treatments. *Trends Neurosci* 30: 357–364, 2007.
- 1011 **Hanslmayr S, Staudigl T, Fellner M-C.** Oscillatory power decreases and long-term memory: the
1012 information via desynchronization hypothesis. *Front Hum Neurosci* 6: 74, 2012.
- 1013 **Hegeman DJ, Hong ES, Hernández VM, Chan CS.** The external globus pallidus: progress and
1014 perspectives. *Eur J Neurosci* 43: 1239–1265, 2016.
- 1015 **Holgado AJN, Terry JR, Bogacz R.** Conditions for the Generation of Beta Oscillations in the

- 1016 Subthalamic Nucleus–Globus Pallidus Network. *J Neurosci* 30, 2010.
- 1017 **Humphries MD, Stewart RD, Gurney KN.** A Physiologically Plausible Model of Action Selection
1018 and Oscillatory Activity in the Basal Ganglia. *J Neurosci* 26: 12921–12942, 2006.
- 1019 **Jávor-Duray BN, Vinck M, van der Roest M, Mulder AB, Stam CJ, Berendse HW, Voorn P.**
1020 Early-onset cortico-cortical synchronization in the hemiparkinsonian rat model [Online]. *J*
1021 *Neurophysiol* 113, 2015. <http://jn.physiology.org.libproxy.ucl.ac.uk/content/113/3/925> [24 Aug.
1022 2017].
- 1023 **Kondabolu K, Roberts EA, Bucklin M, McCarthy MM, Kopell N, Han X.** Striatal cholinergic
1024 interneurons generate beta and gamma oscillations in the corticostriatal circuit and produce motor
1025 deficits. *Proc Natl Acad Sci U S A* 113: E3159-68, 2016.
- 1026 **Koshimizu Y, Fujiyama F, Nakamura KC, Furuta T, Kaneko T.** Quantitative analysis of axon
1027 bouton distribution of subthalamic nucleus neurons in the rat by single neuron visualization with a
1028 viral vector. *J Comp Neurol* 521: 2125–2146, 2013.
- 1029 **Kühn AA, Kupsch A, Schneider G-H, Brown P.** Reduction in subthalamic 8-35 Hz oscillatory
1030 activity correlates with clinical improvement in Parkinson’s disease. *Eur J Neurosci* 23: 1956–60,
1031 2006.
- 1032 **Kumar A, Cardanobile S, Rotter S, Aertsen A.** The role of inhibition in generating and controlling
1033 Parkinson’s disease oscillations in the Basal Ganglia. *Front Syst Neurosci* 5: 86, 2011a.
- 1034 **Kumar A, Cardanobile S, Rotter S, Aertsen A.** The Role of Inhibition in Generating and
1035 Controlling Parkinson’s Disease Oscillations in the Basal Ganglia. *Front Syst Neurosci* 5: 86, 2011b.
- 1036 **Lalo E, Thobois S, Sharott A, Polo G, Mertens P, Pogosyan A, Brown P.** Patterns of Bidirectional
1037 Communication between Cortex and Basal Ganglia during Movement in Patients with Parkinson
1038 Disease. *J Neurosci* 28, 2008.
- 1039 **Lanciego JL, Luquin N, Obeso JA.** Functional neuroanatomy of the basal ganglia. *Cold Spring*
1040 *Harb Perspect Med* 2: a009621, 2012.
- 1041 **Leblois A.** Competition between Feedback Loops Underlies Normal and Pathological Dynamics in
1042 the Basal Ganglia. *J Neurosci* 26: 3567–3583, 2006.
- 1043 **Leblois A, Boraud T, Meissner W, Bergman H, Hansel D.** Competition between Feedback Loops
1044 Underlies Normal and Pathological Dynamics in the Basal Ganglia. *J Neurosci* 26: 3567–3583, 2006.
- 1045 **Levy R.** Dependence of subthalamic nucleus oscillations on movement and dopamine in Parkinson’s
1046 disease. *Brain* 125: 1196–1209, 2002.

- 1047 **Levy R, Hutchison WD, Lozano AM, Dostrovsky JO.** High-frequency Synchronization of
1048 Neuronal Activity in the Subthalamic Nucleus of Parkinsonian Patients with Limb Tremor [Online]. *J*
1049 *Neurosci* 20: 7766–7775, 2000. <http://www.jneurosci.org/content/20/20/7766.full> [21 Oct. 2015].
- 1050 **Lienard JF, Cos I, Girard B.** Beta-Band Oscillations without Pathways: the opposing Roles of D2
1051 and D5 Receptors. *doi.org* (July 10, 2017). doi: 10.1101/161661.
- 1052 **Litvak V, Jha A, Eusebio A, Oostenveld R, Foltynie T, Limousin P, Zrinzo L, Hariz MI, Friston**
1053 **K, Brown P.** Resting oscillatory cortico-subthalamic connectivity in patients with Parkinson’s
1054 disease. *Brain* 134: 359–374, 2011a.
- 1055 **Litvak V, Jha A, Eusebio A, Oostenveld R, Foltynie T, Limousin P, Zrinzo L, Hariz MI, Friston**
1056 **K, Brown P.** Resting oscillatory cortico-subthalamic connectivity in patients with Parkinson’s
1057 disease. *Brain* 134: 359–74, 2011b.
- 1058 **Liu C, Zhu Y, Liu F, Wang J, Li H, Deng B, Fietkiewicz C, Loparo KA.** Neural mass models
1059 describing possible origin of the excessive beta oscillations correlated with Parkinsonian state. *Neural*
1060 *Networks* 88: 65–73, 2017.
- 1061 **López-Azcárate J, Tainta M, Rodríguez-Oroz MC, Valencia M, González R, Guridi J, Iriarte J,**
1062 **Obeso JA, Artieda J, Alegre M.** Coupling between beta and high-frequency activity in the human
1063 subthalamic nucleus may be a pathophysiological mechanism in Parkinson’s disease. *J Neurosci* 30:
1064 6667–77, 2010.
- 1065 **Magill P., Bolam J., Bevan M.** Dopamine regulates the impact of the cerebral cortex on the
1066 subthalamic nucleus–globus pallidus network. *Neuroscience* 106: 313–330, 2001.
- 1067 **Magill PJ, Pogosyan A, Sharott A, Csicsvari J, Bolam JP, Brown P.** Changes in functional
1068 connectivity within the rat striatopallidal axis during global brain activation in vivo. *J Neurosci* 26:
1069 6318–6329, 2006.
- 1070 **Magill PJ, Sharott A, Bolam JP, Brown P.** Brain State–Dependency of Coherent Oscillatory
1071 Activity in the Cerebral Cortex and Basal Ganglia of the Rat [Online]. *J Neurophysiol* 92, 2004.
1072 <http://jn.physiology.org/content/92/4/2122.full> [26 Apr. 2017].
- 1073 **Mallet N, Micklem BR, Henny P, Brown MT, Williams C, Bolam JP, Nakamura KC, Magill PJ.**
1074 Dichotomous Organization of the External Globus Pallidus. *Neuron* 74: 1075–1086, 2012.
- 1075 **Mallet N, Pogosyan A, Marton LF, Bolam JP, Brown P, Magill PJ.** Parkinsonian Beta Oscillations
1076 in the External Globus Pallidus and Their Relationship with Subthalamic Nucleus Activity. *J*
1077 *Neurosci* 28: 14245–14258, 2008a.
- 1078 **Mallet N, Pogosyan A, Sharott A, Csicsvari J, Bolam JP, Brown P, Magill PJ.** Disrupted

- 1079 Dopamine Transmission and the Emergence of Exaggerated Beta Oscillations in Subthalamic Nucleus
1080 and Cerebral Cortex. *J Neurosci* 28: 4795–4806, 2008b.
- 1081 **Marceglia S, Foffani G, Bianchi AM, Baselli G, Tamma F, Egidi M, Priori A.** Dopamine-
1082 dependent non-linear correlation between subthalamic rhythms in Parkinson’s disease. *J Physiol* 571:
1083 579–591, 2006.
- 1084 **Maris E.** Statistical testing in electrophysiological studies. *Psychophysiology* 49: 549–565, 2012.
- 1085 **Maris E, Oostenveld R.** Nonparametric statistical testing of EEG- and MEG-data. *J Neurosci*
1086 *Methods* 164: 177–190, 2007.
- 1087 **Marreiros AC, Cagnan H, Moran RJ, Friston KJ, Brown P.** Basal ganglia–cortical interactions in
1088 Parkinsonian patients. *Neuroimage* 66: 301–310, 2013.
- 1089 **Matias FS, Carelli P V., Mirasso CR, Copelli M.** Anticipated synchronization in a biologically
1090 plausible model of neuronal motifs. *Phys Rev E* 84: 21922, 2011.
- 1091 **McCarthy MM, Moore-Kochlacs C, Gu X, Boyden ES, Han X, Kopell N.** Striatal origin of the
1092 pathologic beta oscillations in Parkinson’s disease. *Proc Natl Acad Sci U S A* 108: 11620–5, 2011.
- 1093 **McHaffie JG, Stanford TR, Stein BE, Coizet V, Redgrave P.** Subcortical loops through the basal
1094 ganglia. *Trends Neurosci* 28: 401–407, 2005.
- 1095 **Medkour T, Walden AT, Burgess A.** Graphical modelling for brain connectivity via partial
1096 coherence. *J Neurosci Methods* 180: 374–383, 2009.
- 1097 **van der Meer M, Kalenscher T, Lansink CS, Pennartz C, Berke JD, Redish AD.** Integrating early
1098 results on ventral striatal gamma oscillations in the rat. *Front Neurosci* 4: 300, 2010.
- 1099 **Moran RJ, Mallet N, Litvak V, Dolan RJ, Magill PJ, Friston KJ, Brown P.** Alterations in brain
1100 connectivity underlying beta oscillations in parkinsonism. *PLoS Comput Biol* 7: e1002124, 2011.
- 1101 **Nambu A, Tokuno H, Takada M.** Functional significance of the cortico–subthalamo–pallidal
1102 “hyperdirect” pathway. *Neurosci Res* 43: 111–117, 2002.
- 1103 **Nevado-Holgado AJ, Mallet N, Magill PJ, Bogacz R.** Effective connectivity of the subthalamic
1104 nucleus - globus pallidus network during Parkinsonian oscillations. *J Physiol* 7: 1429–1455, 2014.
- 1105 **Ni Z, Bouali-Benzzouz R, Gao D, Benabid A-L, Benazzouz A.** Changes in the firing pattern of
1106 globus pallidus neurons after the degeneration of nigrostriatal pathway are mediated by the subthalamic
1107 nucleus in the rat. *Eur J Neurosci* 12: 4338–4344, 2000.
- 1108 **Nicolás MJ, López-Azcárate J, Valencia M, Alegre M, Pérez-Alcázar M, Iriarte J, Artieda J.**
1109 Ketamine-Induced Oscillations in the Motor Circuit of the Rat Basal Ganglia. *PLoS One* 6: e21814,

- 1110 2011.
- 1111 **Nolte G, Bai O, Wheaton L, Mari Z, Vorbach S, Hallett M.** Identifying true brain interaction from
1112 EEG data using the imaginary part of coherency. *Clin Neurophysiol* 115: 2292–307, 2004.
- 1113 **Oostenveld R, Fries P, Maris E, Schoffelen J-M, Oostenveld R, Fries P, Maris E, Schoffelen J-**
1114 **M.** FieldTrip: Open Source Software for Advanced Analysis of MEG, EEG, and Invasive
1115 Electrophysiological Data. *Comput Intell Neurosci* 2011: 1–9, 2011.
- 1116 **Oswal A, Beudel M, Zrinzo L, Limousin P, Hariz M, Foltynie T, Litvak V, Brown P.** Deep brain
1117 stimulation modulates synchrony within spatially and spectrally distinct resting state networks in
1118 Parkinson’s disease. *Brain* 139: 1482–1496, 2016.
- 1119 **Parker PRL, Lalive AL, Kreitzer AC.** Pathway-Specific Remodeling of Thalamostriatal Synapses
1120 in Parkinsonian Mice. *Neuron* 89: 734–740, 2016.
- 1121 **Pavlidis A, Hogan SJ, Bogacz R.** Computational Models Describing Possible Mechanisms for
1122 Generation of Excessive Beta Oscillations in Parkinson’s Disease. *PLOS Comput Biol* 11: e1004609,
1123 2015.
- 1124 **Pavlidis A, John Hogan S, Bogacz R.** Improved conditions for the generation of beta oscillations in
1125 the subthalamic nucleus-globus pallidus network. *Eur J Neurosci* 36: 2229–2239, 2012.
- 1126 **Paxinos G, Watson C.** *The rat brain in stereotaxic coordinates*. Elsevier, 2007.
- 1127 **Plenz D, Kital ST.** A basal ganglia pacemaker formed by the subthalamic nucleus and external
1128 globus pallidus. *Nature* 400: 677–82, 1999.
- 1129 **Priori A, Foffani G, Pesenti A, Tamma F, Bianchi AM, Pellegrini M, Locatelli M, Moxon KA,**
1130 **Villani RM.** Rhythm-specific pharmacological modulation of subthalamic activity in Parkinson’s
1131 disease. *Exp Neurol* 189: 369–79, 2004.
- 1132 **Qiu C, Shivacharan RS, Zhang M, Durand DM.** Can Neural Activity Propagate by Endogenous
1133 Electrical Field? *J Neurosci* 35: 15800–11, 2015.
- 1134 **Ray NJ, Jenkinson N, Wang S, Holland P, Brittain JS, Joint C, Stein JF, Aziz T.** Local field
1135 potential beta activity in the subthalamic nucleus of patients with Parkinson’s disease is associated
1136 with improvements in bradykinesia after dopamine and deep brain stimulation. *Exp Neurol* 213: 108–
1137 113, 2008.
- 1138 **Rosenberg JR, Halliday DM, Breeze P, Conway BA.** Identification of patterns of neuronal
1139 connectivity—partial spectra, partial coherence, and neuronal interactions. *J Neurosci Methods* 83:
1140 57–72, 1998.

- 1141 **Salvador R, Suckling J, Schwarzbauer C, Bullmore E.** Undirected graphs of frequency-dependent
1142 functional connectivity in whole brain networks. *Philos Trans R Soc Lond B Biol Sci* 360: 937–46,
1143 2005.
- 1144 **Sato F, Parent M, Levesque M, Parent A.** Axonal branching pattern of neurons of the subthalamic
1145 nucleus in primates. *J Comp Neurol* 424: 142–152, 2000.
- 1146 **Schnitzler A, Gross J.** Normal and pathological oscillatory communication in the brain. *Nat Rev*
1147 *Neurosci* 6: 285–96, 2005.
- 1148 **Schoffelen J-M, Oostenveld R, Fries P.** Neuronal coherence as a mechanism of effective
1149 corticospinal interaction. *Science* 308: 111–113, 2005.
- 1150 **Schroll H, Hamker FH.** Computational models of basal-ganglia pathway functions: focus on
1151 functional neuroanatomy. *Front Syst Neurosci* 7: 1–18, 2013.
- 1152 **Schroll H, Vitay J, Hamker FH.** Dysfunctional and compensatory synaptic plasticity in Parkinson’s
1153 disease. *Eur J Neurosci* 39: 688–702, 2014.
- 1154 **Schwartzing RK, Huston JP.** Unilateral 6-hydroxydopamine lesions of meso-striatal dopamine
1155 neurons and their physiological sequelae. [Online]. *Prog Neurobiol* 49: 215–66, 1996a.
1156 <http://www.ncbi.nlm.nih.gov/pubmed/8878304> [28 Apr. 2017].
- 1157 **Schwartzing RK, Huston JP.** The unilateral 6-hydroxydopamine lesion model in behavioral brain
1158 research. Analysis of functional deficits, recovery and treatments. [Online]. *Prog Neurobiol* 50: 275–
1159 331, 1996b. <http://www.ncbi.nlm.nih.gov/pubmed/8971983> [28 Apr. 2017].
- 1160 **Sharott A, Gulberti A, Zittel S, Tudor Jones AA, Fickel U, Münchau A, Köppen JA, Gerloff C,**
1161 **Westphal M, Buhmann C, Hamel W, Engel AK, Moll CKE.** Activity Parameters of Subthalamic
1162 Nucleus Neurons Selectively Predict Motor Symptom Severity in Parkinson’s Disease [Online]. *J*
1163 *Neurosci* 34, 2014. <http://www.jneurosci.org.libproxy.ucl.ac.uk/content/34/18/6273> [24 Aug. 2017].
- 1164 **Sharott A, Magill PJ, Bolam JP, Brown P.** Directional analysis of coherent oscillatory field
1165 potentials in the cerebral cortex and basal ganglia of the rat. *J Physiol* 562: 951–63, 2005a.
- 1166 **Sharott A, Magill PJ, Harnack D, Kupsch A, Meissner W, Brown P.** Dopamine depletion
1167 increases the power and coherence of beta-oscillations in the cerebral cortex and subthalamic nucleus
1168 of the awake rat. *Eur J Neurosci* 21: 1413–1422, 2005b.
- 1169 **Sharott A, Moll CKE, Engler G, Denker M, Grün S, Engel AK.** Different Subtypes of Striatal
1170 Neurons Are Selectively Modulated by Cortical Oscillations [Online]. *J Neurosci* 29, 2009.
1171 <http://www.jneurosci.org/content/29/14/4571.long> [24 Jul. 2017].
- 1172 **Sharott A, Vinciati F, Nakamura KC, Magill PJ.** A Population of Indirect Pathway Striatal

- 1173 Projection Neurons Is Selectively Entrained to Parkinsonian Beta Oscillations. *J Neurosci* 37: 9977–
1174 9998, 2017.
- 1175 **Shen W, Flajolet M, Greengard P, Surmeier DJ.** Dichotomous Dopaminergic Control of Striatal
1176 Synaptic Plasticity [Online]. *Science* (80-) 321, 2008.
1177 <http://science.sciencemag.org/content/321/5890/848.long> [23 Jun. 2017].
- 1178 **Shouno O, Tachibana Y, Nambu A, Doya K.** Computational Model of Recurrent Subthalamo-
1179 Pallidal Circuit for Generation of Parkinsonian Oscillations. *Front Neuroanat* 11: 21, 2017.
- 1180 **Smith Y, Bevan MD, Shink E, Bolam JP.** Microcircuitry of the direct and indirect pathways of the
1181 basal ganglia. *Neuroscience* 86: 353–387, 1998.
- 1182 **Smith Y, Galvan A, Ellender TJ, Doig N, Villalba RM, Huerta-Ocampo I, Wichmann T, Bolam**
1183 **JP.** The thalamostriatal system in normal and diseased states. *Front Syst Neurosci* 8: 5, 2014.
- 1184 **Stam CJ, Nolte G, Daffertshofer A.** Phase lag index: Assessment of functional connectivity from
1185 multi channel EEG and MEG with diminished bias from common sources. *Hum Brain Mapp* 28:
1186 1178–1193, 2007.
- 1187 **Steriade M.** Corticothalamic resonance, states of vigilance and mentation. *Neuroscience* 101: 243–
1188 276, 2000.
- 1189 **Tachibana Y, Iwamuro H, Kita H, Takada M, Nambu A.** Subthalamo-pallidal interactions
1190 underlying parkinsonian neuronal oscillations in the primate basal ganglia. *Eur J Neurosci* 34: 1470–
1191 1484, 2011.
- 1192 **Terman D, Rubin JE, Yew AC, Wilson CJ.** Activity patterns in a model for the subthalamopallidal
1193 network of the basal ganglia. *J Neurosci* 22: 2963–2976, 2002.
- 1194 **Thut G, Miniussi C, Gross J.** The functional importance of rhythmic activity in the brain. *Curr Biol*
1195 22: R658-63, 2012.
- 1196 **Tseng KY, Kasanetz F, Kargieman L, Riquelme LA, Murer MG.** Cortical Slow Oscillatory
1197 Activity Is Reflected in the Membrane Potential and Spike Trains of Striatal Neurons in Rats with
1198 Chronic Nigrostriatal Lesions [Online]. *J Neurosci* 21, 2001.
1199 <http://www.jneurosci.org/content/21/16/6430.long> [2 May 2017].
- 1200 **Uhlhaas PJ, Singer W.** Neural Synchrony in Brain Disorders: Relevance for Cognitive Dysfunctions
1201 and Pathophysiology. *Neuron* 52: 155–168, 2006.
- 1202 **Varela F, Lachaux J-PP, Rodriguez E, Martinerie J.** The brainweb: phase synchronization and
1203 large-scale integration. *Nat Rev Neurosci* 2: 229–39, 2001.

- 1204 **Vicente R, Gollo LL, Mirasso CR, Fischer I, Pipa G.** Dynamical relaying can yield zero time lag
1205 neuronal synchrony despite long conduction delays. *Proc Natl Acad Sci U S A* 105: 17157–62, 2008.
- 1206 **Vinck M, Oostenveld R, van Wingerden M, Battaglia F, Pennartz CMA.** An improved index of
1207 phase-synchronization for electrophysiological data in the presence of volume-conduction, noise and
1208 sample-size bias. *Neuroimage* 55: 1548–1565, 2011.
- 1209 **Viriopase A, Bojak I, Zeitler M, Gielen S.** When Long-Range Zero-Lag Synchronization is
1210 Feasible in Cortical Networks. *Front Comput Neurosci* 6: 49, 2012.
- 1211 **Weinberger M, Mahant N, Hutchison WD, Lozano AM, Moro E, Hodaie M, Lang AE,**
1212 **Dostrovsky JO.** Beta oscillatory activity in the subthalamic nucleus and its relation to dopaminergic
1213 response in Parkinson’s disease. *J Neurophysiol* 96: 3248–56, 2006.
- 1214 **West T, Farmer S, Berthouze L, Jha A, Beudel M, Foltynie T, Limousin P, Zrinzo L, Brown P,**
1215 **Litvak V.** The Parkinsonian Basal Ganglia Network: Measures of Power, Linear and Non-Linear
1216 Synchronization and their Relationship to L-DOPA Treatment and OFF State Motor Severity. *Front*
1217 *Hum Neurosci* 10: 517, 2016.
- 1218 **Whitmer D, de Solages C, Hill B, Yu H, Henderson JM, Bronte-Stewart H.** High frequency deep
1219 brain stimulation attenuates subthalamic and cortical rhythms in Parkinson’s disease. *Front Hum*
1220 *Neurosci* 6: 155, 2012.
- 1221 **Wichmann T, DeLong MR.** Neurobiology: Oscillations in the basal ganglia. *Nature* 400: 621–622,
1222 1999.
- 1223 **van Wijk BCM, Neumann W-J, Schneider G-H, Sander TH, Litvak V, Kühn AA.** Low-beta
1224 cortico-pallidal coherence decreases during movement and correlates with overall reaction time.
1225 *Neuroimage* (2017). doi: 10.1016/j.neuroimage.2017.07.024.
- 1226 **Wilson CJ.** Active decorrelation in the basal ganglia. *Neuroscience* 250: 467–482, 2013.
- 1227 **Zold CL, Kasanetz F, Pomata PE, Belluscio MA, Escande M V, Galinanes GL, Riquelme LA,**
1228 **Murer MG.** Striatal gating through up states and oscillations in the basal ganglia: Implications for
1229 Parkinson’s disease. *J Physiol Paris* 106: 40–6, 2012.
- 1230 Figure Legends:
- 1231 Figure 1 – **Cortical-basal ganglia circuits and experimental paradigm.** (A) Schematic of
1232 canonical cortical-basal ganglia circuit incorporating the antagonistic direct and indirect pathways
1233 first described by Albin et al. (1989), as well as the cortico-subthalamic hyperdirect pathway (Nambu
1234 et al., 2002). The motor cortex (M2, purple) has major inputs to the basal ganglia at the striatum
1235 (STR, green) and subthalamic nucleus (STN, red). Information flow along the indirect pathway is

1236 routed via the external segment of the globus pallidus (GPe, Orange). Both indirect, direct and
1237 hyperdirect pathways ultimately impinge upon the output nuclei of the basal ganglia, made up of the
1238 entopeduncular nucleus (EPN) and substantia nigra pars reticulata (SNr). BG output targets thalamic
1239 relays, of which some return back to motor cortex. Brain structures from which neuronal signals were
1240 recorded in this study are delineated by solid boxes, with solid arrows indicating their connections
1241 (interactions) that were analyzed here. Other structures and interactions are respectively delineated by
1242 dashed boxes and arrows. **(B)** Diagram of the recording configuration in anaesthetised rats. Local
1243 field potentials (LFPs) were recorded from the BG using two multi-channel ‘silicon probes’; the first
1244 probe was targeted to the STR and GPe, whereas the second probe was targeted to STN.
1245 Electroencephalograms (EEG) were recorded with a screw positioned over the “secondary motor
1246 cortex” (M2). Boundaries and positioning are approximate.

1247 **Figure 2 - Example recordings of subcortical monopolar LFP and cortical ECoG signals for a**
1248 **single animal from either the control (A-B), or the 6-OHDA lesioned (C-D) groups. (A)** 100
1249 second sample of LFPs recording made from one dopamine intact, control animal. The example trace
1250 shows the time course of LFP recordings recorded using silicon electrodes implanted in the external
1251 globus pallidus (GPe), striatum (STR) and subthalamic nucleus (STN). Additionally, ECoG was
1252 recorded from a screw positioned over motor cortex (M2). Only raw data is shown. The data was de-
1253 meaned and then high pass filtered at 4Hz. **(B)** Spectral analysis of example control animal’s
1254 recording. Data was epoched into 1-second long segments, those contaminated by muscle artefact or
1255 high amplitude transients were removed using Z-thresholding as described in the text. These epochs
1256 were used to construct individual FFTs and subsequent periodograms. **(C)** Same as (A) but for an
1257 example 6-OHDA, dopamine depleted animal. The dashed line shows a regression to estimate the 1/f
1258 background noise. **(D)** Same as (B) but for 6-OHDA lesioned animal.

1259 **Figure 3 – Group averaged power spectra for all rats across both control and lesion conditions.**
1260 Spectra are shown for signals recorded from **(A)** motor cortex (M2), **(B)** the striatum (STR), **(C)** the
1261 subthalamic nucleus (STN), and **(D)** the external globus pallidus (GPe). The group averages for either
1262 the 6-OHDA dopamine depleted or control animals are shown by bold lines in red or blue
1263 respectively. Shading shows the mean ± 1 S.E.M. Results of cluster permutation tests for the effect of
1264 the lesion are indicated by the black bar and corresponding P-value. All recording sites presented beta
1265 peaks around 18-20 Hz. Cluster based permutation testing for significant differences between
1266 conditions showed that there was a significant increase in beta in the lesioned animals for signals at all
1267 recorded sites. The dashed lines indicate a linear regression in log-log space as a rough estimate to the
1268 1/f background.

1269 **Figure 4 – Functional connectivity estimates using imaginary part of coherence (iCOH).** Spectra
1270 for each animal are shown by thin lines corresponding to either 6-OHDA lesioned (blue) or control

1271 (red). The group averages for either the 6-OHDA dopamine depleted or control animals are shown by
1272 bold lines in red or blue respectively. Shading shows the mean ± 1 S.E.M. Cluster-based permutation
1273 statistics were applied to test the effect of the lesion. Significant clusters are indicated by the black
1274 line above the spectra and corresponding P-value. The iCOH metric, robust to zero-lag interactions,
1275 presents a richer view of functional connectivity that would otherwise be missed if using standard
1276 coherence (data not shown). Beta activity is predominant across all cross-regional pairings. STN and
1277 GPe also show intra-nuclear correlations in this range in the dopamine depleted state. Notably there is
1278 also a high beta/gamma interaction between STN/M2 and STN/STR that is visible in both control and
1279 lesion animals.

1280 **Figure 5 - Directed connectivity estimated using non-parametric directionality (NPD) between**
1281 **subcortically recorded LFPs (GPe, STN, and STR) and ECoG recorded at motor cortex (M2).**
1282 NPD decomposes the coherence between pairs of signals into forward and reverse components. The
1283 array of spectra in the figures reads such that each row title gives the structure with a forward
1284 coherence targeted to the structure given by the name given above the column. The group averages for
1285 either the 6-OHDA dopamine depleted or control animals are shown by bold lines in red or blue
1286 respectively. Shading shows the mean ± 1 S.E.M. Cluster-based permutation statistics were applied to
1287 test the effect of the lesion. Significant clusters are indicated by the black line above the spectra and
1288 corresponding P-value.

1289 **Figure 6 - Non-parametric directionality conditioned on the STN local field potential - Spectra**
1290 for each animal are shown by thin lines corresponding to either 6-OHDA lesioned (blue) or control
1291 (red). The group averages for either the 6-OHDA dopamine depleted or control animals are shown by
1292 bold lines in red or blue respectively. Shading shows the mean ± 1 S.E.M. Cluster-based permutation
1293 statistics were applied to test the effect of the lesion. Significant clusters are indicated by the black
1294 line above the spectra and corresponding P-value. The effect of conditioning with the STN LFP was
1295 also tested using cluster permutation statistics. Frequencies where NPD was significantly attenuated
1296 by the conditioning are indicated by the red and blue bars (and corresponding P-values) for the control
1297 and lesion recordings respectively.

1298 **Figure 7 - Non-parametric directionality conditioned on the GPe local field potential - Spectra for**
1299 for each animal are shown by thin lines corresponding to either 6-OHDA lesioned (blue) or control (red).
1300 The group averages for either the 6-OHDA dopamine depleted or control animals are shown by bold
1301 lines in red or blue respectively. Shading shows the mean ± 1 S.E.M. Cluster-based permutation
1302 statistics were applied to test the effect of the lesion. Significant clusters are indicated by the black
1303 line above the spectra and corresponding P-value. The effect of conditioning with the GPe LFP was
1304 also tested using cluster permutation statistics. Frequencies where NPD was significantly attenuated

1305 by the conditioning are indicated by the red and blue bars (and corresponding P-values) for the control
1306 and lesion recordings respectively.

1307 Figure 8 - **Non-parametric directionality conditioned on the STR local field potential** - Spectra
1308 for each animal are shown by thin lines corresponding to either 6-OHDA lesioned (blue) or control
1309 (red). The group averages for either the 6-OHDA dopamine depleted or control animals are shown by
1310 bold lines in red or blue respectively. Shading shows the mean ± 1 S.E.M. Cluster-based permutation
1311 statistics were applied to test the effect of the lesion. Significant clusters are indicated by the black
1312 line above the spectra and corresponding P-value. The effect of conditioning with the STR LFP was
1313 also tested using cluster permutation statistics. Frequencies where NPD was significantly attenuated
1314 by the conditioning are indicated by the red and blue bars (and corresponding P-values) for the control
1315 and lesion recordings respectively.

1316 Figure 9 - **Non-parametric directionality conditioned on the M2 electrocorticogram** - Spectra for
1317 each animal are shown by thin lines corresponding to either 6-OHDA lesioned (blue) or control (red).
1318 The group averages for either the 6-OHDA dopamine depleted or control animals are shown by bold
1319 lines in red or blue respectively. Shading shows the mean ± 1 S.E.M. Cluster-based permutation
1320 statistics were applied to test the effect of the lesion. Significant clusters are indicated by the black
1321 line above the spectra and corresponding P-value. The effect of conditioning with the M2 ECoG was
1322 also tested using cluster permutation statistics. Frequencies where NPD was significantly attenuated
1323 by the conditioning are indicated by the red and blue bars (and corresponding P-values) for the control
1324 and lesion recordings respectively.

1325 Table 1– **Summary of hypotheses of the impact of dopamine depletion on the propagation of**
1326 **beta rhythms in the cortico-basal ganglia circuit.**

1327 Table 2 – **Summary of hypotheses for gamma flow in the cortico-basal ganglia circuit**

1328

1329

1330

1331

1332

1333

1334

1335

1336

1337

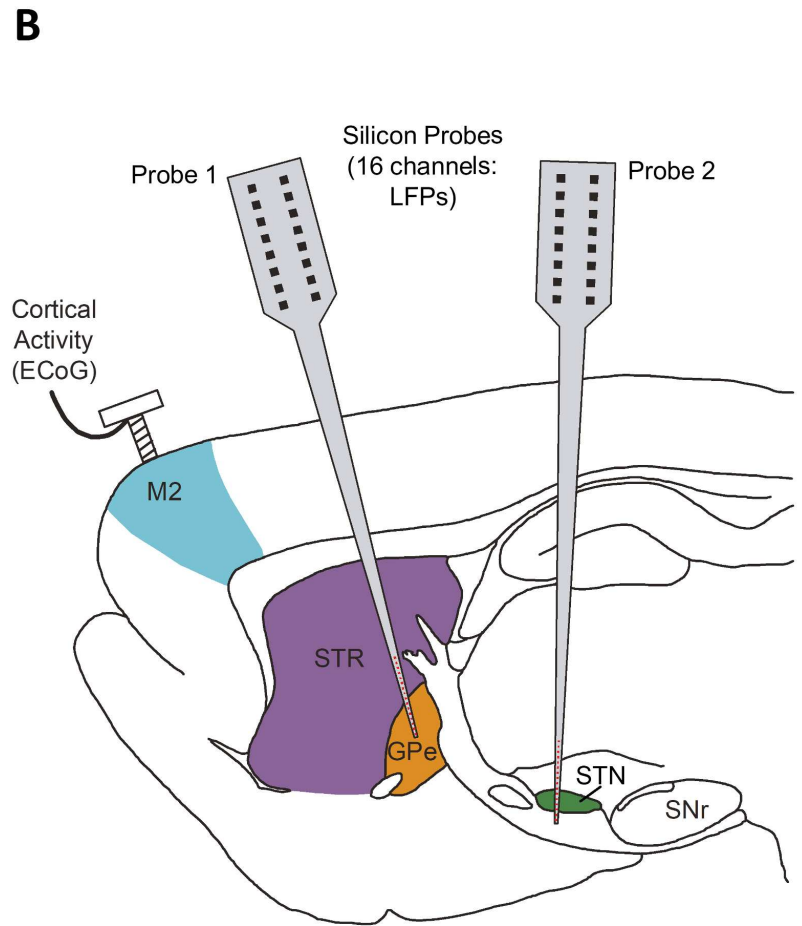
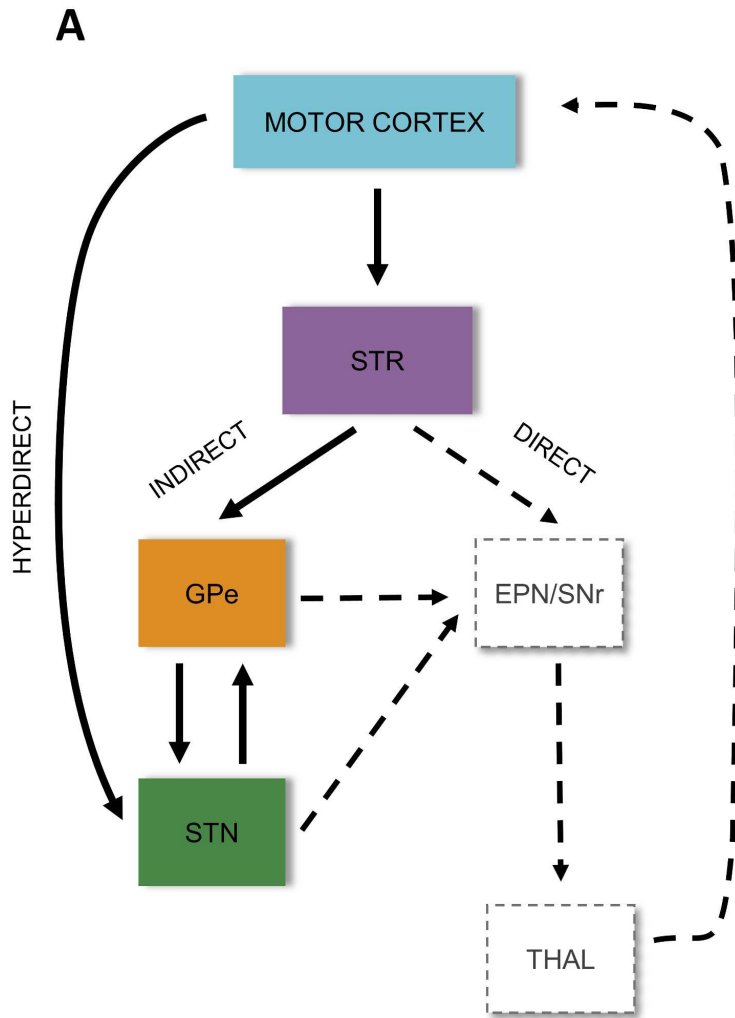
1338

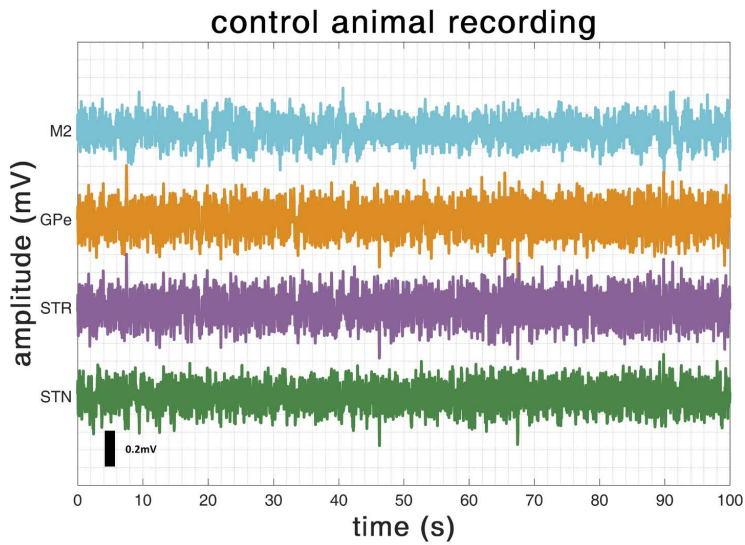
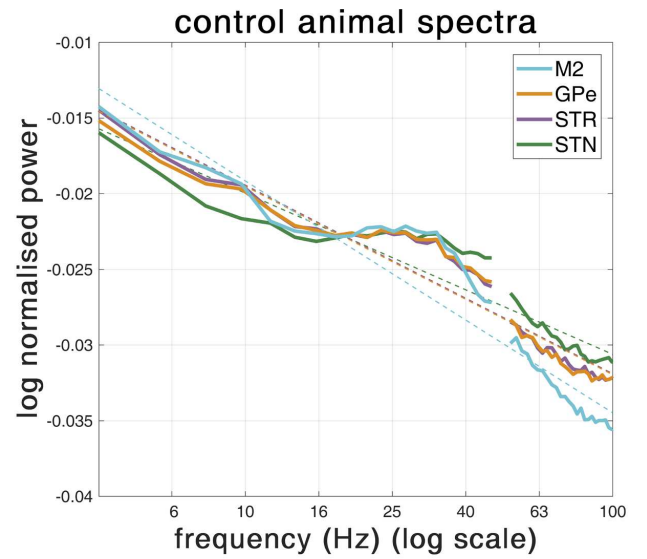
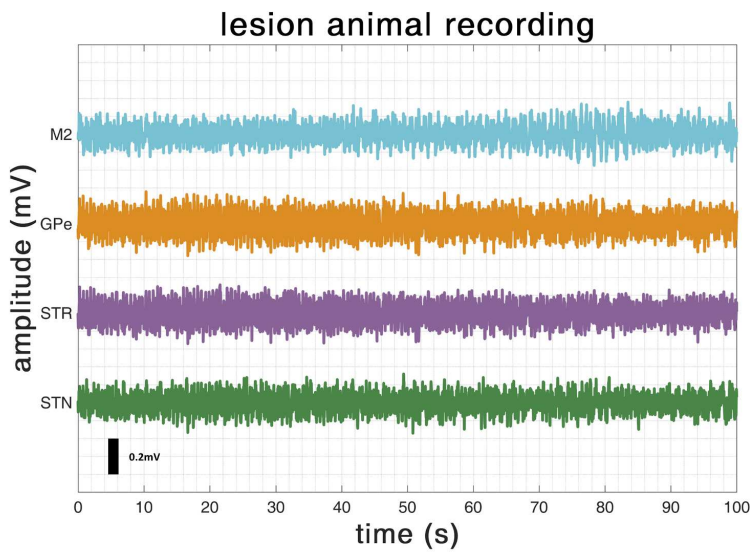
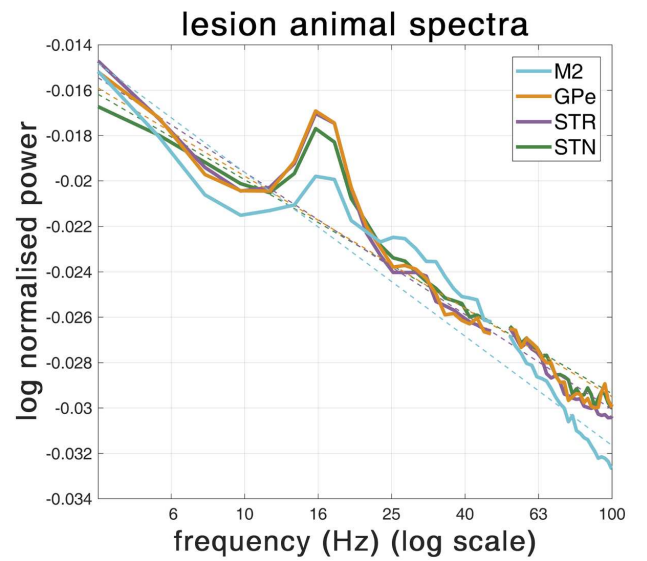
1339

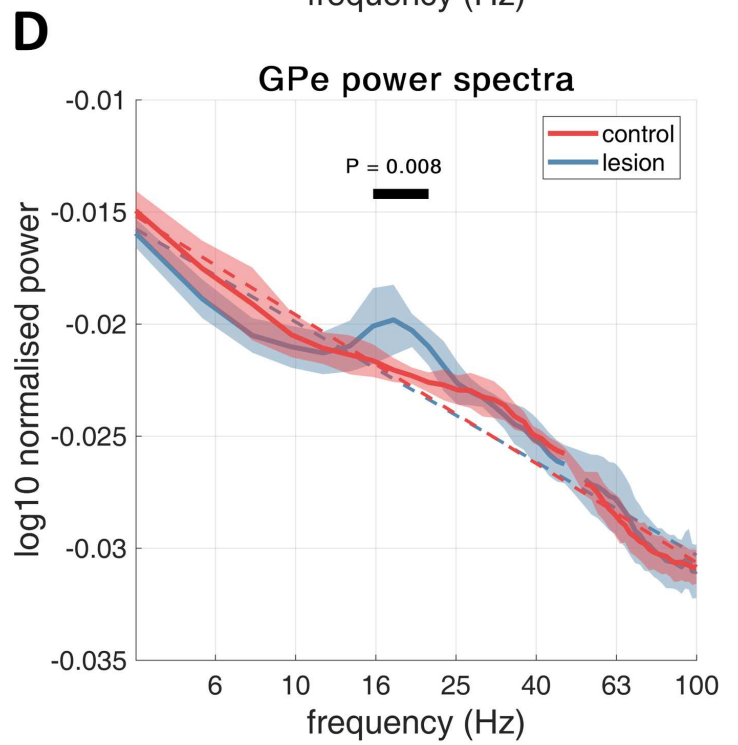
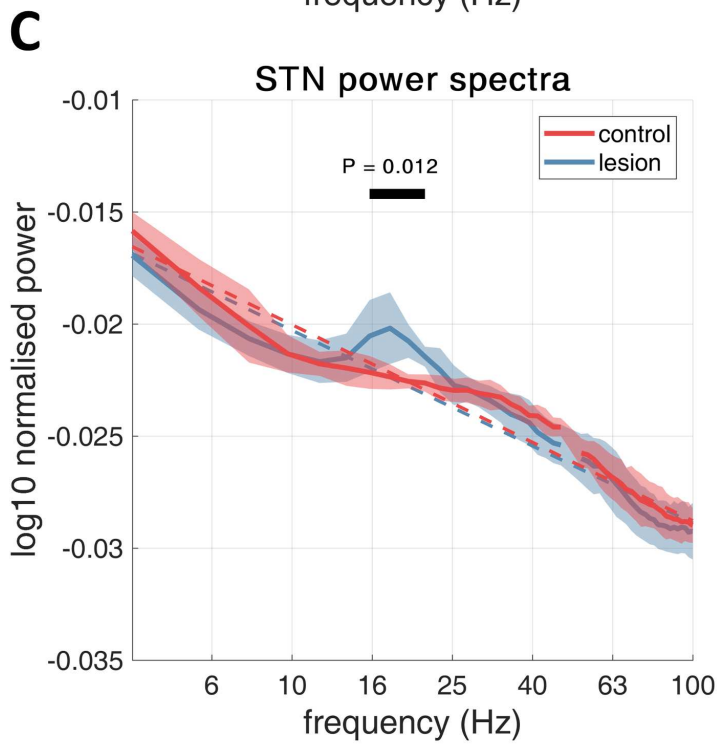
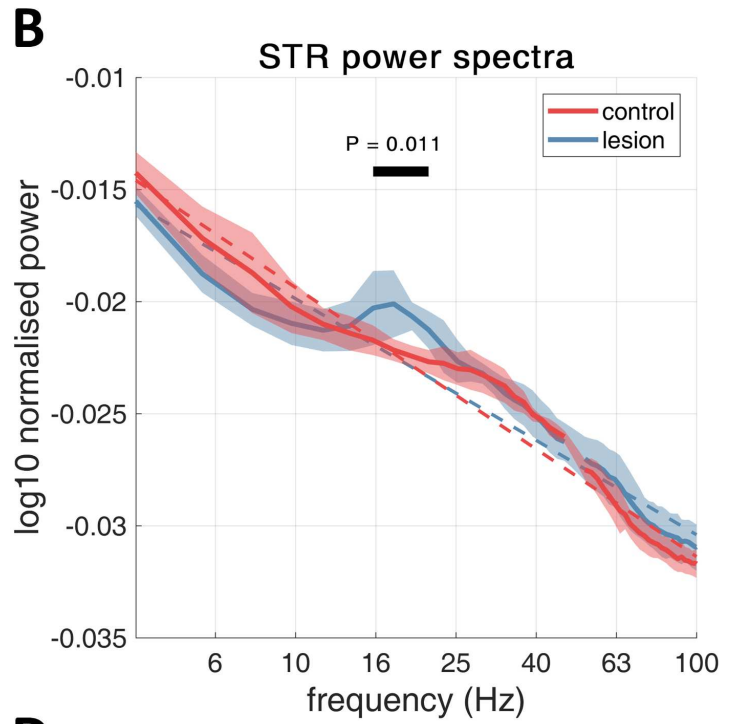
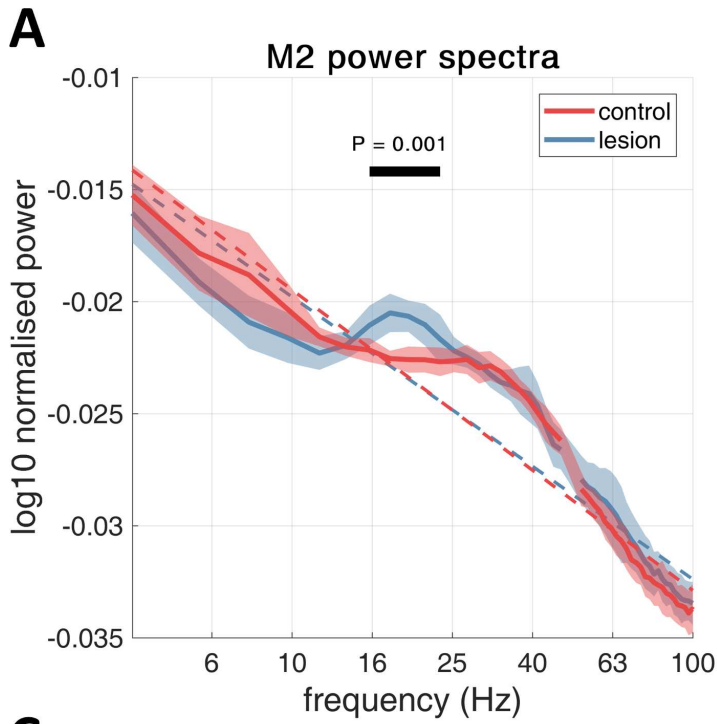
1340

1341

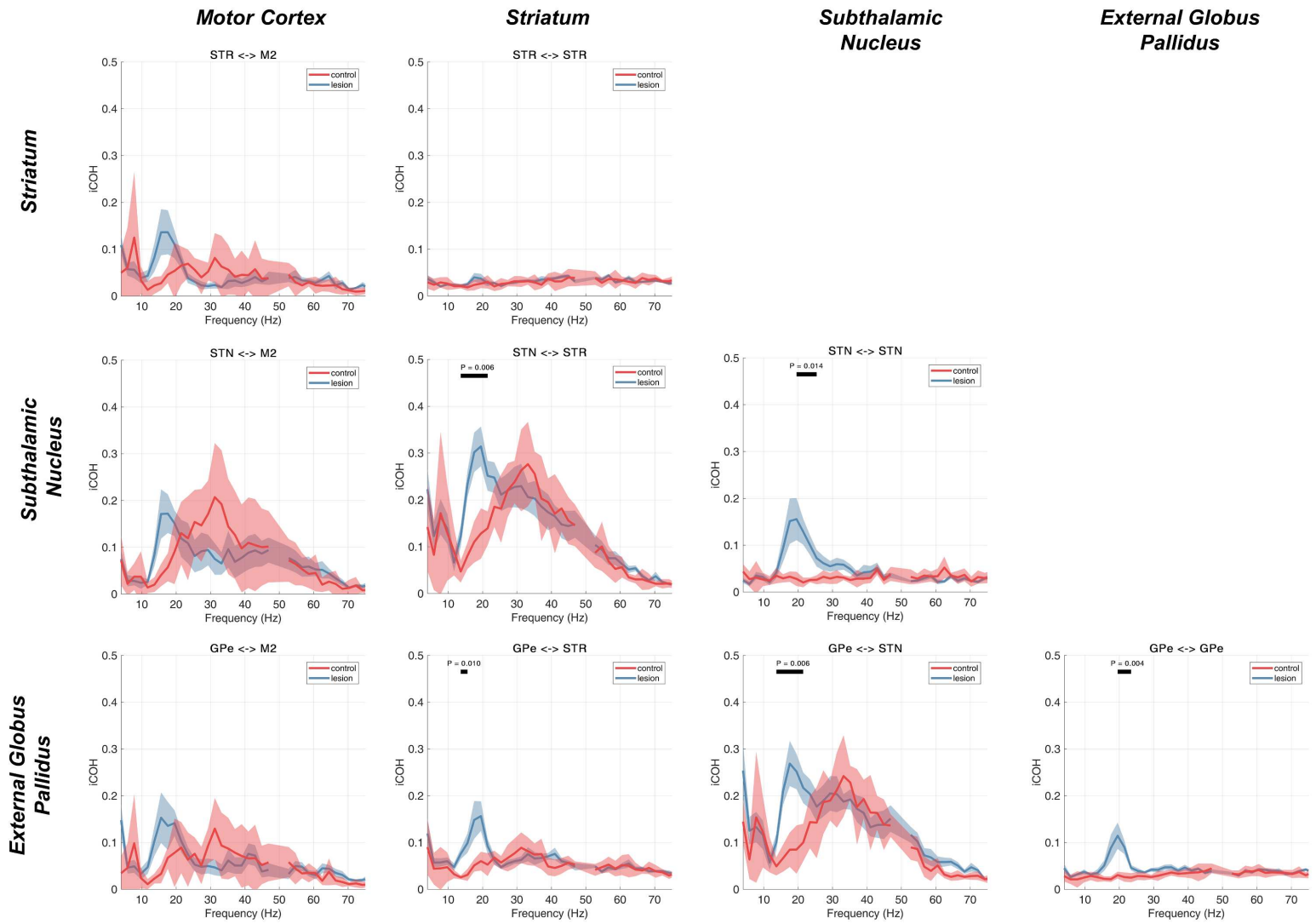
1342



A**B****C****D**



Imaginary Coherence



TO

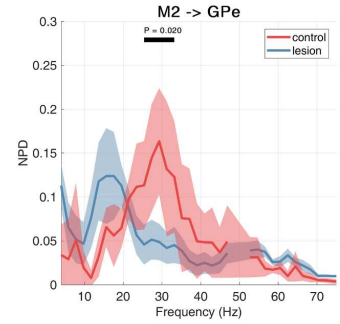
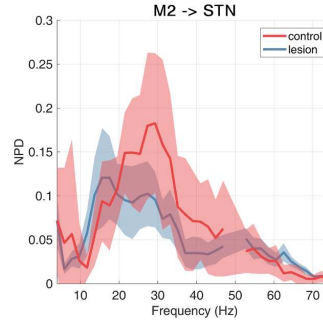
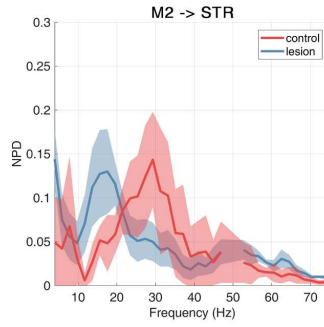
Motor Cortex

Striatum

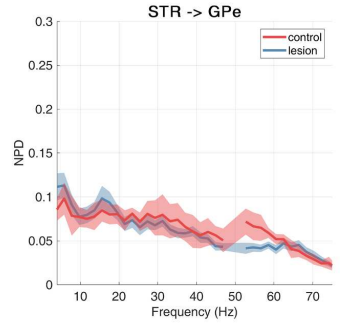
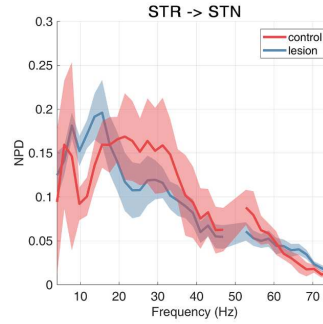
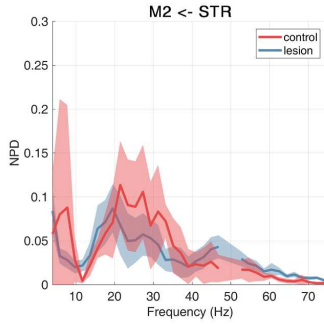
Subthalamic Nuclei

External Globus Pallidus

Motor Cortex

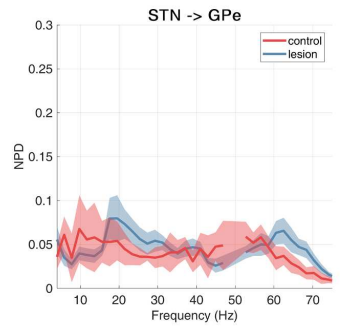
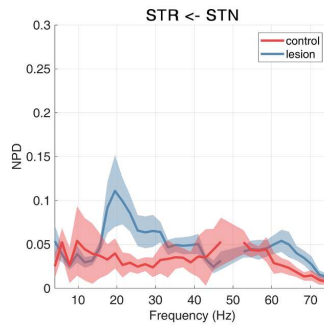
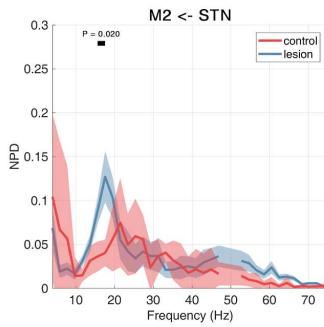


Striatum

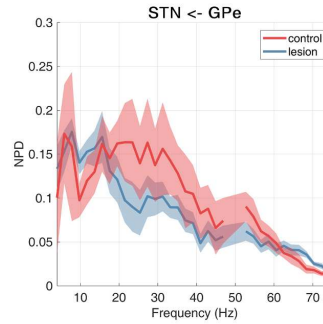
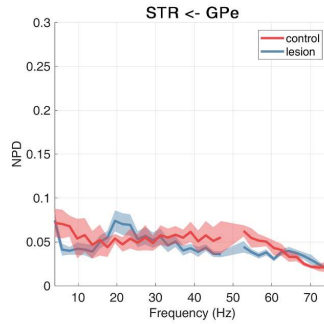
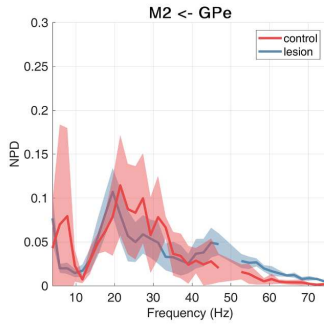


FROM

Subthalamic Nuclei



External Globus Pallidus



Non-Parametric Directionality

FROM

Motor Cortex

Striatum

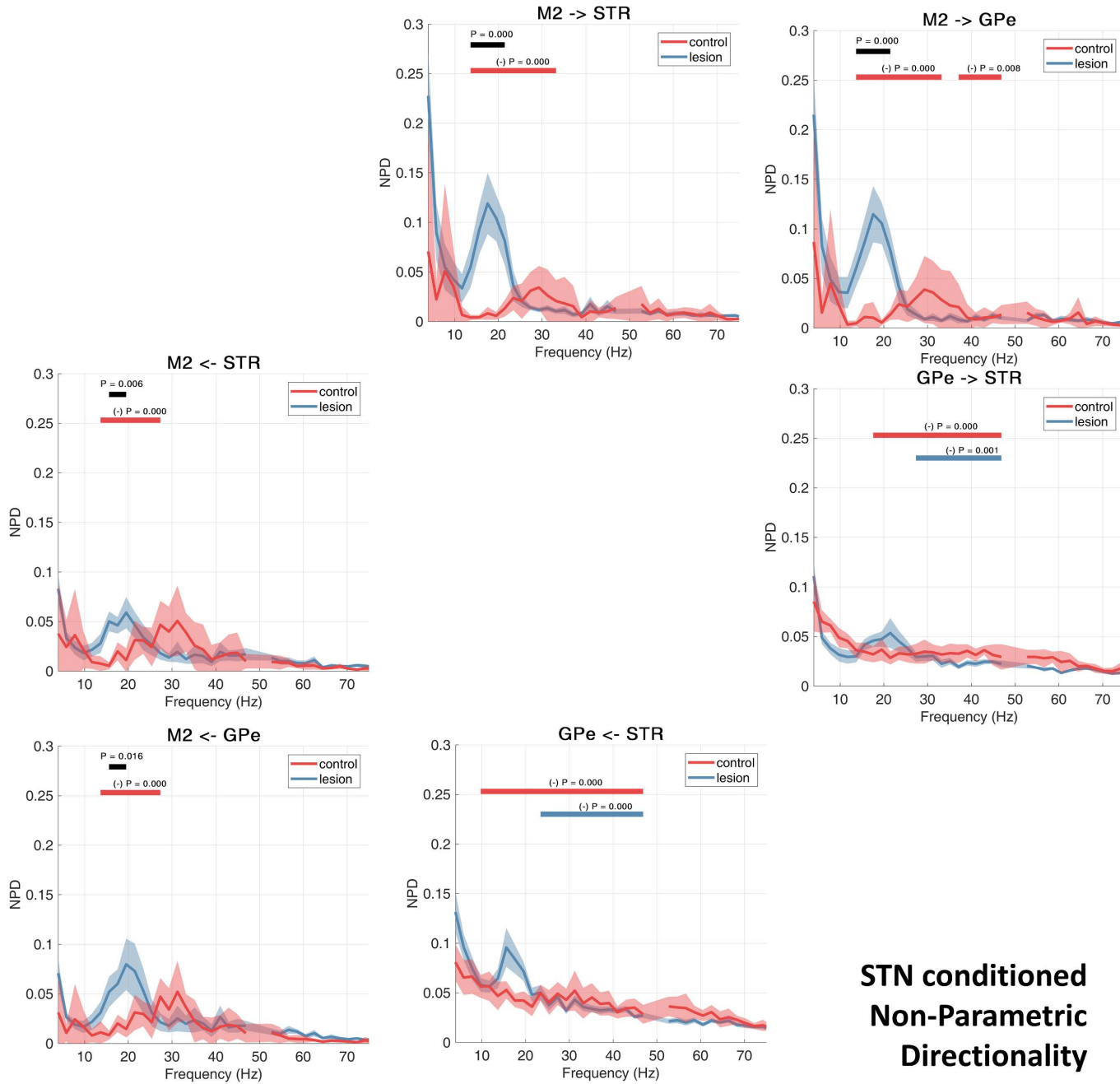
External Globus
Pallidus

TO

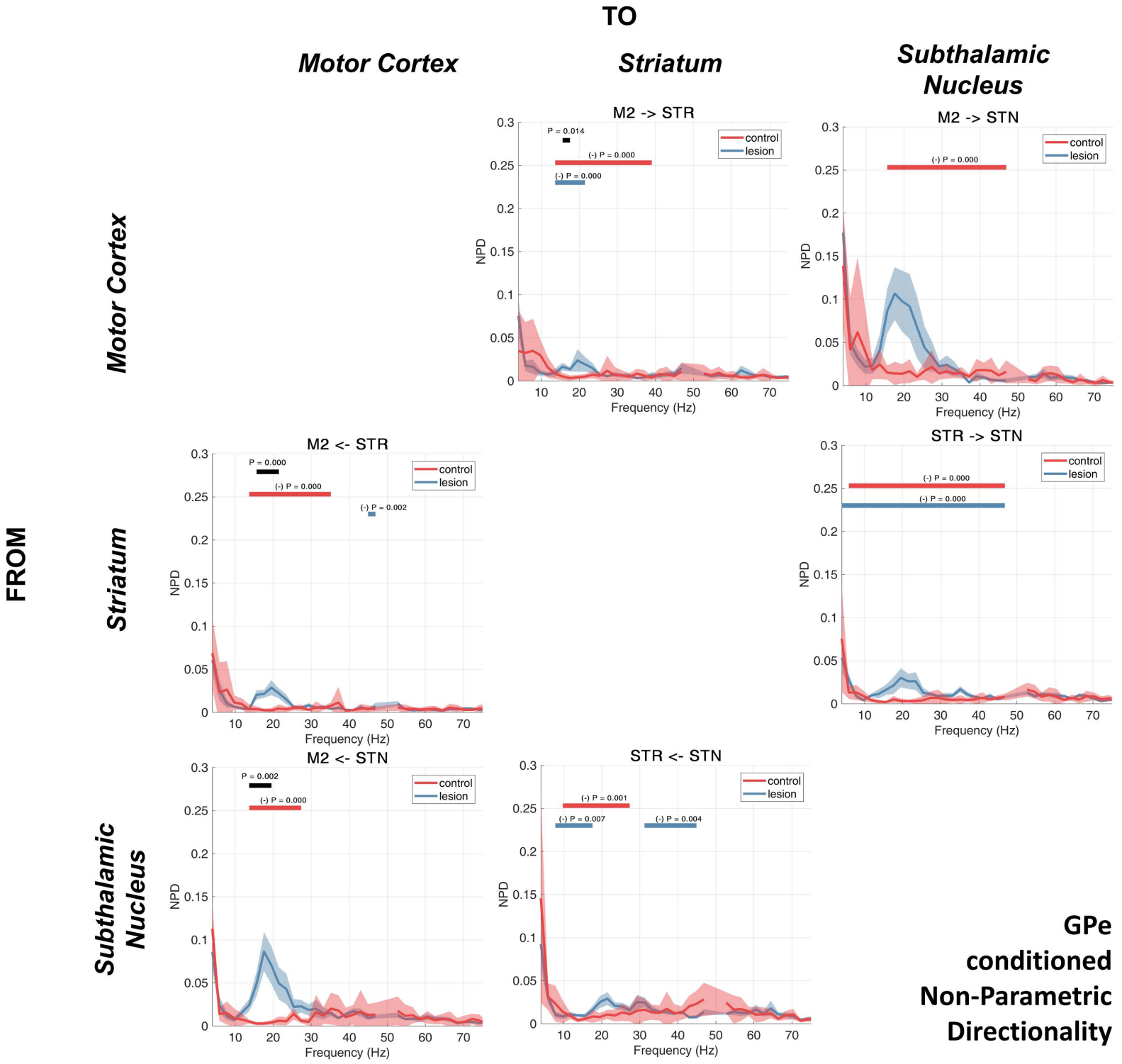
Motor Cortex

Striatum

External Globus
Pallidus



STN conditioned
Non-Parametric
Directionality



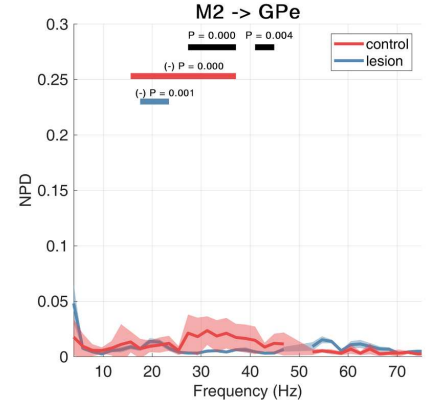
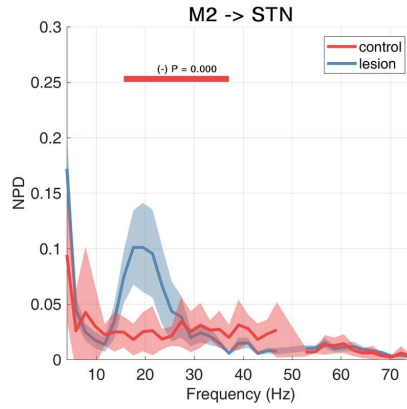
TO

Motor Cortex

Subthalamic Nucleus

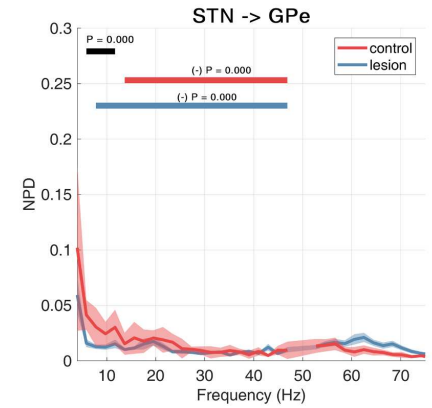
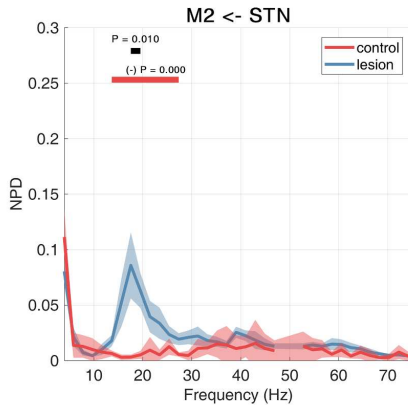
External Globus Pallidus

Cortex

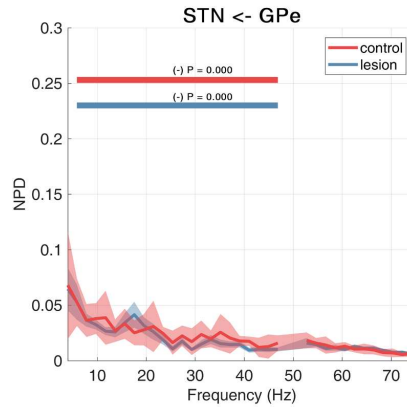
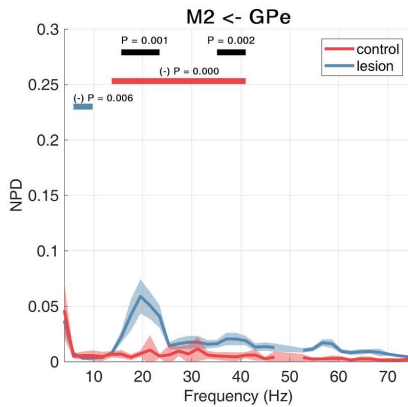


FROM

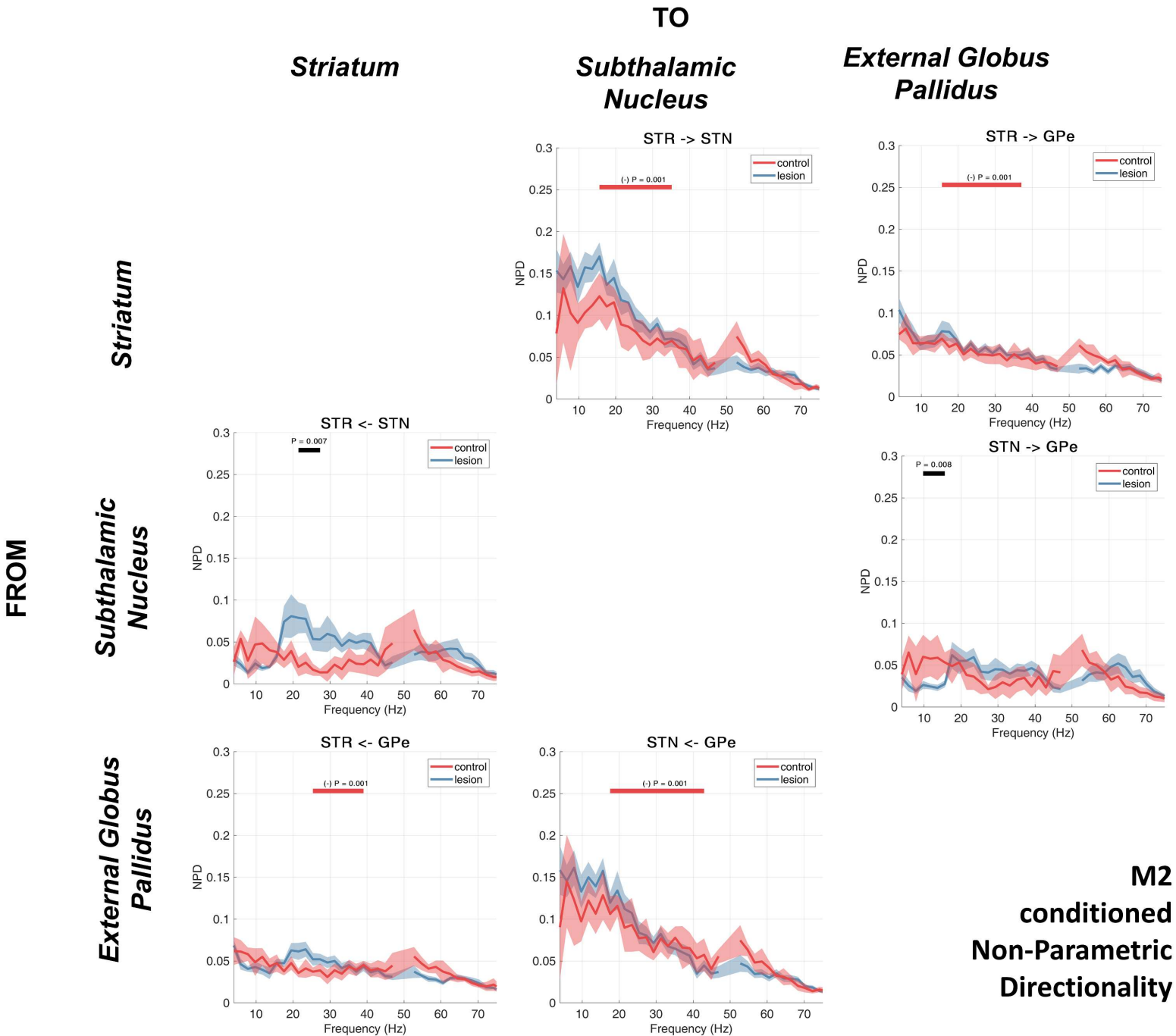
Subthalamic Nucleus



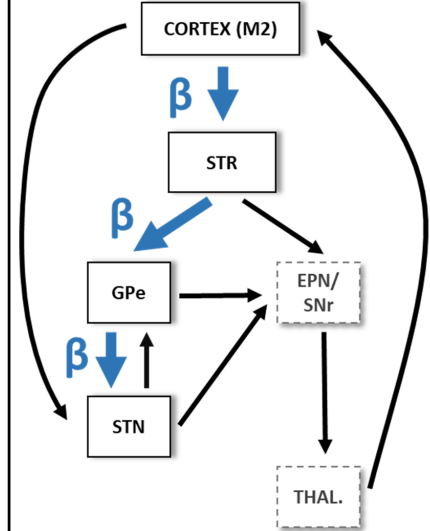
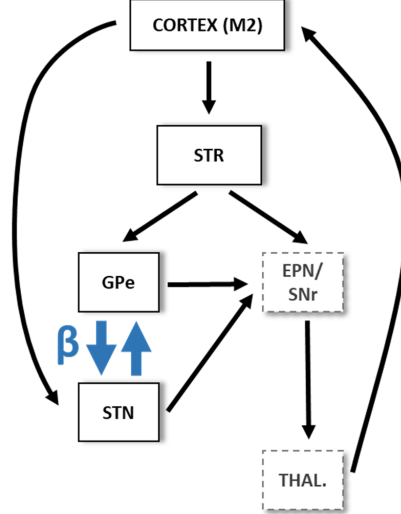
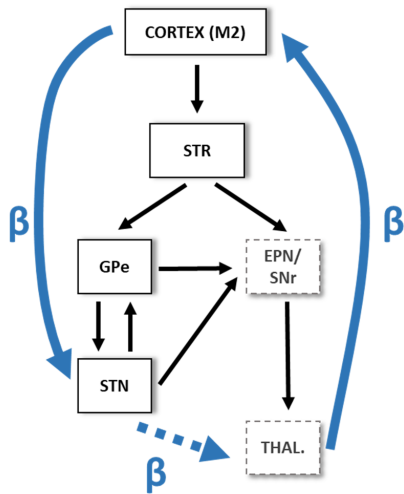
External Globus Pallidus



STR
conditioned
Non-Parametric
Directionality



Hypotheses for propagation of low beta rhythms



Mechanism:

“Long-loop” resonance

STN/GPe Resonance Pair

Aberrant (cortico-) striatal output

Pathological beta arises from induction of a loop formed by feedback between cortex and BG

Pathological beta arises from increased coupling of STN/GPe resonance pair.

Pathological beta results from changed internal dynamics of STR and/or its outputs to the indirect pathway.

Evidence for:

- Significant beta band STN/M2 NPD in both the forward and reverse directions.
- The low beta STN → M2 feedback coherence is significantly increased in the lesioned animals.
- STN/M2 NPD is undiminished by conditioning with GPe or STR.

- iCOH of the STN↔GPe suggests coupling increases in 6-OHDA experiments.
- The STN → GPe NPD is not attenuated by conditioning with the M2 ECoG.

- STN↔GPe NPDs are strongly attenuated by conditioning with STR signals.
- Conditioning of the STR → GPe NPD with the M2 ECoG is only effective in the control animals.
- Conditioning of the STR → GPe NPD with the STN LFPs is only effective in the control animals.

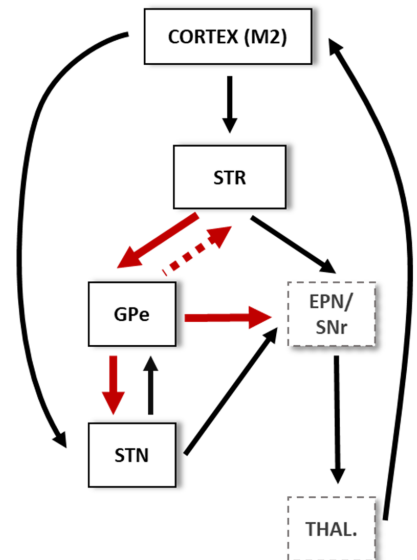
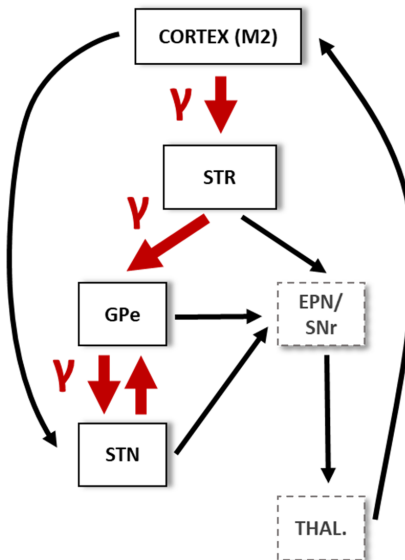
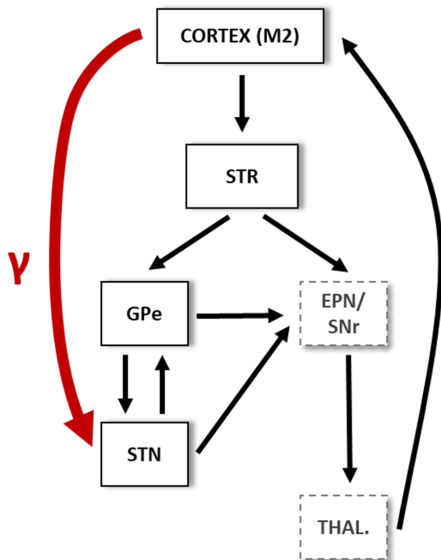
Evidence against:

- Conditioning the NPD with signals from the STN or M2 does not remove beta band NPD between STR and GPe, upstream of the STN.
- No test to determine routing of return signal from STN to cortex.

- There is a strong asymmetry in between the forward and backwards STN↔GPe NPDs, suggesting pallidal drive is dominant.
- The STN↔GPe NPDs are strongly attenuated by conditioning with the STR signal.
- Conditioning NPDs with the STN signal has little effect on coupling upstream in the indirect pathway.

- Unclear whether lack of effect of conditioning is due to change in the STR output or due to change to STN signal such as that occurring due to increased hyperdirect input described in hypothesis (1).

Hypotheses for propagation of high beta/gamma rhythms



Mechanism:

Hyper-direct inflow

**Cortico-striatal
gamma input**

Subcortical generator

High beta/gamma enters the subcortical network via the hyper-direct M2→STN connection.

Cortical-gamma enters the BG via the striatum and is passed down the indirect pathway.

High beta/gamma arises from subcortical interactions and/or local dynamics within BG nuclei

Evidence for:

- iCOH shows that M2 ↔ STR interaction is much weaker than the M2 ↔ STN.
- Conditioning subcortical NPDs with ECoG attenuates a large number of connections.

- Conditioning subcortical NPDs with ECoG attenuates a large number of connections.
- Conditioning of the M2 → STN NPD with STR or GPe attenuates interactions in the control condition suggesting signal is passed via striatal-pallidal projections.
- NPD conditioned by the STN is less effective for interactions upstream in the indirect pathway.

- Conditioning of NPDs using signals from STR or GPe reduces strength of interactions.
- Conditioning of STN→STR NPD with ECoG does not act to remove subthalamo-striatal feedback suggesting existence of subcortical feedback.

Evidence against:

- Conditioning of the M2→STN NPD with STR or GPe signals attenuates interactions in the control conditions.

- Conditioning of STN→STR NPD with ECoG does not act to remove subthalamo-striatal feedback suggesting existence of subcortical feedback.

- No evidence for within STR interaction from iCOH.